

Changes in Kuroshio Current dynamics and East Asian monsoon variability during the last 26 kyr

Fenies Pierrick ^{1,*}, Bassetti Maria-Angela ¹, Vazquez Riveiros Natalia ², Menniti Christophe ¹, Frigola Clément ^{3,4}, Babonneau Nathalie ⁹, Ratzov Gueorgui ⁵, Hsu Shu-Kun ^{6,7}, Su Chih-Chieh ⁸

¹ CEFREM, Université de Perpignan Via Domitia, UMR 5110, CEDEX, 52 Avenue Paul Alduy, Perpignan 66860, France

² Geo-Ocean, UMR 6538, CNRS-Ifremer-UBO-UBS, France

³ LUSAC, Université de Caen Normandie, Cherbourg-en-Cotentin, France

⁴ Conservatoire National des Arts et Métiers, INTECHMER, Cherbourg-en-Cotentin, France

⁵ Université Côte d'Azur, CNRS, Observatoire de la Côte d'Azur, IRD, Géoazur, Nice, France

⁶ Department of Earth Sciences, National Central University, Taoyuan, 32001, Taiwan

⁷ Institute of Earth Sciences, Academia Sinica, Taipei 11529, Taiwan

⁸ National Taiwan University, Institute of Oceanography, 1, Sec. 4, Roosevelt Road, Taipei City 106, Taiwan, ROC

⁹ Geo-Ocean, UMR 6538, CNRS-Ifremer-UBO-UBS, France

* Corresponding author : Pierrick Fenies, email address : pie.fenies@gmail.com

Abstract :

The Kuroshio Current flows northward along the east coast of Taiwan toward the Okinawa Trough and the East China Sea, but its dynamics and trajectory were probably different during the Last Glacial Maximum (LGM) due to the globally lower sea level that could have caused a (debated) deflection of the current along the eastern edge of the Ryukyu Arc.

Core MD18–3532 has been recovered in an intra-slope basin of the Ryukyu accretionary prism, currently disconnected from the Kuroshio Current, but would have been on its trajectory in case of a NE deflection. Measurements of clay mineral assemblages and illite crystallinity revealed that Taiwan has been the main sediment source at this site over the last 26 kyr. The significantly higher sedimentation rate from the Last Glacial Maximum to the Bølling–Allerød compared with the period from the Younger Dryas to the Holocene, coupled with very low $\delta^{15}\text{N}_{\text{sed}}$ during LGM and Heinrich Stadial 1, provide evidence for the transport of sediments and *Trichodesmium* spp. cyanobacteria by the partially deflected Kuroshio Current toward the eastern edge of the Ryukyu Arc. Combined with $\delta^{13}\text{C}_{\text{org}}$, TOC, TN, and XRF analyses, an increase in primary productivity has been observed during LGM and Heinrich Stadial 1. This would have been caused by an enhanced East Asian Winter monsoon winds resulting in the deepening of the mixed layer that would have led to the upwelling of the Kuroshio Current nutrient-enriched subsurface waters to the oligotrophic surface waters, and the supply of dust-borne iron from the Chinese Loess Plateau.

Highlights

► The Kuroshio Current deflected partially eastward during the LGM and HS1. ► The Kuroshio Current exerts a strong control on the dispersion of hypopycnal flows. ► Dust and upwelled nutrients under intensified EAWM control paleoproductivity. ► Intensified primary productivity in the NW Philippine Sea during the LGM and HS1.

Keywords : Kuroshio Current deflection, NW Philippine Sea, Taiwan paleoceanography, primary productivity, last deglaciation, *Trichodesmium* spp.

1 Introduction

The Kuroshio Current is the western boundary current of the North Pacific Subtropical Gyre. It flows northward along the eastern coast of East Asia (Fig. 1a), transferring heat, salinity and moisture from the Indo Pacific Warm Pool to the high latitudes. While its surface water is oligotrophic, marked by low concentration of chlorophyll-a (Chen et al., 2022) reflecting reduced phytoplanktonic activity, the Kuroshio Current transports large quantities of nutrients on the subsurface (300 – 600 m; maximum core of the nutrient flux at 400 – 500 m depth) (Chen et al., 2017; Guo et al., 2012). It is also at the origin of a “water barrier” effect in the East China Sea preventing the export of sediments from Chinese rivers (e.g. Yangtze River) to the Okinawa Trough during summer. This “water barrier” effect decreases during the winter, enhancing the export of sediments to the Okinawa Trough (Zheng et al., 2016).

As a result of this transfer of heat and moisture, the Kuroshio Current has a major impact on global scale by regulating the thermal balance between low and high latitudes, and on regional scale by regulating local climate and ocean dynamics (Hu et al., 2015). The gradual intensification of the Kuroshio Current over the deglaciation under the influence of East Asian Monsoon changes and the El Niño Southern Oscillation is well established (Li et al., 2020; Lim et al., 2017; Zheng et al., 2016; Zou et al., 2021). However, over the past two decades, the Kuroshio Current has been the subject of debate (Li et al., 2020; Lim et al., 2017; Ujiie and Ujiie, 1999; Vogt-Vincent and Mitarai, 2020; Wang et al., 2015; Zheng et al., 2016) regarding whether it was still able to flow through the Yonaguni Depression and remain in the Okinawa Trough, or whether it was deflected eastwards along the eastern edge of the Ryukyu Arc, as a result of the ~130 m drop in sea level (Lambeck et al., 2014)

during the Last Glacial Maximum (LGM; 23.0 – 19.0 thousands of years ago; ka afterwards) (Mix et al., 2001). At glacial/interglacial and stadial/interstadial scale, the deflection of the Kuroshio Current pathway out of the Okinawa Trough may affect East Asia and the East China Sea through changes in East Asian Summer Monsoon (EASM) rainfall patterns (Sasaki et al., 2012), the range of East Asian Winter Monsoon (EAWM) winds propagation (Pan et al., 2018), the ability of typhoons to sustain themselves with the heat and moisture of the surface ocean (Fujiwara et al., 2020; He et al., 2022; Liu and Wei, 2015; Wu et al., 2008), and through primary productivity changes outside and inside the Okinawa Trough (Chen, 2000).

Previous studies based on planktonic foraminifera (Ujiié and Ujiié, 1999; Ujiié et al., 2003), clay mineral analysis (Diekmann et al., 2008; Dou et al., 2010) and Sr-Nd isotopes (Dou et al., 2012) suggest a complete deflection of the Kuroshio Current from the Okinawa Trough toward the eastern edge of the Ryukyu Arc during LGM and its return to the Okinawa Trough since at least 14 ka. Other studies using geochemical (Lim et al., 2017; Xu et al., 2019), mineralogical (Li et al., 2019), paleotemperature proxies (Kim et al., 2015; Li et al., 2020) and modeling results (Vogt-Vincent and Mitarai, 2020; Zheng et al., 2016) suggest that the Kuroshio Current did not deflect and would have persisted, albeit weakly, in the Okinawa Trough during the low sea level period, beginning to strengthen since ~14 ka.

These previous studies are mainly based on sediments collected in the Okinawa Trough, and little attention has so far been paid to the northwestern Philippine Sea, south of the Ryukyu Arc (Fig. 1a), where deflection, if any, would have occurred. To fill this gap, in this study we analyze sediment core MD18-3532, located in an intra-slope basin of the Ryukyu accretionary prism in the northwest Philippine Sea (Fig. 1b). This core is currently

disconnected from the Kuroshio Current, but might have been on its pathway during the low sea level period if it had deflected eastward.

The Kuroshio Current carries sediments delivered to the surface waters by eastern Taiwanese rivers (Diekmann et al., 2008; Dou et al., 2012; Li et al., 2019; Wang et al., 2015). A change in the amount and/or source of sediment could therefore be an indicator of the deflection of the Kuroshio Current or a weakening of its “barrier effect” that prevents the offshore export of sediments from Taiwan (Fig. 1b). Also, the emergence of the East China Sea shelf during the glacial low sea level drove the migration of the Yangtze River mouth across the shelf to the border of the Okinawa Trough, with those sediments being carried directly into the Okinawa Trough (Dou et al., 2012, 2010; Li et al., 2019) and possibly to the Ryukyu accretionary wedge area, becoming an additional sediment sources. Finally, enhanced EAWM during LGM and Heinrich Stadial 1 (HS1; 18.0 – 14.7 ka) (Denton et al., 2010) might have transported dust from Chinese Loess Plateau to the Philippine Sea as evidenced by previous studies (Jiang et al., 2016; Wan et al., 2012; Xu et al., 2015). Therefore, in order to constrain potential changes in sediment supply and sources, we have investigated the provenance of the sediments by using clay minerals and illite crystallinity as sediment source indicators (Dou et al., 2010; Li et al., 2012; Nayak et al., 2021) and sedimentation rate variability.

In addition, the Kuroshio Current is well-known to carry abundant *Trichodesmium* spp. cyanobacteria (Chen et al., 2008; Shiozaki et al., 2015), characteristic of its oligotrophic surface waters (Chen et al., 1995; Kodama et al., 2014), that generate significant nitrogen fixation compared to the rest of the Philippine Sea (Liu et al., 1996; Shiozaki et al., 2015). Therefore, we have also used sedimentary $\delta^{15}\text{N}$ ($\delta^{15}\text{N}_{\text{sed}}$) to reconstruct changes in nitrogen

fixation that might indicate a deflection of the Kuroshio Current rather than a weakening of its “barrier effect”.

Finally, the Kuroshio Current transports nutrients to the subsurface which when brought to the surface lead to the increase in primary productivity (Chen et al., 2022; Chen, 2000). During Marine Isotope Stage 2 (MIS 2; 27.8 – 14.7 ka; Sanchez Goñi and Harrison, 2010), the combination of a deflected Kuroshio Current with enhanced EAWM winds might have increase the primary productivity by supplying dust-borne iron to the study area and deepening the mixed layer, causing upwelling of Kuroshio Current nutrient-rich subsurface water. Therefore, using organic and inorganic geochemical proxies (TOC, TN, $\delta^{15}\text{N}_{\text{sed}}$, $\delta^{13}\text{C}_{\text{org}}$, Br/Al, Ti/Al and Fe/Al) combined with previous geochemical proxies, we investigate changes in the paleoproductivity in the northwestern Philippine Sea that might indicate the partial deflection of the Kuroshio Current.

2 General setting

Taiwan is located along the Eurasian margin (Fig. 1a), between 21°54'N and 25°18'N, and is climatically under the influence of the EASM and typhoons (Chen and Chen, 2003; Chen et al., 2010) that generate in the West Pacific Warm Pool (Gray, 1977). The hydrological regime is characterised by heavy rainfall comprised between 1500 – 2500 mm yr⁻¹, reaching 5000 mm yr⁻¹ in the north and north-east of Taiwan (Li et al., 2013; Resentini et al., 2017). The large surrection rate (5 – 20 mm yr⁻¹; Ching et al., 2011; Hsu et al., 2018) is compensated by an average erosion rate of 1 to 10 mm yr⁻¹ over the whole island, which can reach 30 to 60 mm yr⁻¹ locally (Dadson et al., 2003). This erosion causes an important and rapid export of sediments to the ocean by hypopycnal and hyperpycnal flows (Dadson et al., 2005; Mulder et al., 2003) that reach 208 to 332 Mt yr⁻¹, including 68.5 (± 35.4) ($\pm 2\sigma$); as all the $\pm\text{SD}$

hereafter) Mt yr^{-1} through the north-eastern rivers of Taiwan (Lanyang – Hualian rivers) (Resentini et al., 2017). This results in high sedimentation rates in the coastal regions of Taiwan of few hundred cm kyr^{-1} (see supplementary materials) (Li et al., 2009; Wei et al., 2005; Yu et al., 2017). High sedimentation rates are also observed in the western mud area of the East China Sea shelf ($100 - 300 \text{ cm kyr}^{-1}$) related to the transport of sediments from the Yangtze River (480 Mt yr^{-1} ; Xu et al., 2007) and, to a lesser extent, transport of the Taiwanese rivers (Dong et al., 2020).

North East Taiwan, in the region of the Ryukyu accretionary prism, hyperpycnal flows pass through the Hopping Canyon to the Nanao Basin (Fig. 1b) (3700 m below sea level or b.s.l.). These flows possibly do not cross the submarine morphological barrier of the Nanao Rise (3 400 m b.s.l.). The absence of pyrrhotite, a characteristic mineral of the Central Range (Horng et al., 2012), in the sediments of the East Nanao Basin (Hsiung et al., 2017), supports this assumption. Moreover, a reduced occurrence of turbidites in the East Nanao Basin (4 600 m b.s.l.) compared to the Nanao Basin has been observed (Nayak et al., 2021). Generally speaking, the finest sediment fraction of turbidity flows may remain in suspension and cross over topographic ridges of hundreds of meters (Kneller and Buckee, 2000). However, the Yaeyama Ridge (2 800 m b.s.l.), a barrier separating the East Nanao Basin and the MD18-3532 basin, is about 1 800 m high (Fig. S1 in Supplementary Material), too high for allowing the totality of the turbidity flows to cross the obstacle, that could be partial at the most and transporting only the finest silts, isolating the intra-slope basins from sedimentary inputs from Taiwan and the Ryukyu Arc (Fig. 1b) (Hsiung et al., 2017). The sediments constituting the hypopycnal flows are diverted to the Okinawa Trough by the Kuroshio Current (Fig. 1a).

The Kuroshio Current emerges from the bifurcation of the North Equatorial Current, between 8 and 17°N (Qiu et al., 2015) and flows northward along Philippines and Taiwan eastern coasts before entering the Okinawa Trough in the East China Sea through the Yonaguni Depression (sill depth ± 775 m) (Qiu, 2001) and the Kerama Gap (sill depth ± 1100 m) (Na et al., 2014). It exits the East China Sea through the Tokara Strait (sill depth ± 690 m) (Qiu, 2001) and joins the North Pacific (Fig. 1a). Nowadays, east of Taiwan, the Kuroshio Current transports a volume of 11 – 23 Sv ($1 \text{ Sv} = 10^6 \text{ m}^3 \text{ s}^{-1}$) for a maximum current velocity between 0.7 and 1.4 m s^{-1} (Jan et al., 2015). Its boundary can be delimited by the 0.2 m s^{-1} marine isotach at 30 m depth based on historical ADCP data set (Jan et al., 2015). Within these limits, its width is between 85 and 135 km for a thickness of 400 to 600 m, centred at 122°E (Jan et al., 2015).

Below 600 m, the intermediate waters flow northwards but at a speed of less than 0.2 m s^{-1} . When they reach the Ilan Ridge, which bridges Taiwan and the Ryukyu Arc and constitutes the bottom of the Yonaguni Depression, the intermediate waters are deflected eastward, along the eastern edge of the Ryukyu Island, forming the Ryukyu Current (Wang et al., 2019) (Fig. 1a). It exhibits a main core with a velocity maximum of 0.2 to 0.1 m s^{-1} between 600 and 1000 m depth (Wang et al., 2019). East of the Kuroshio Current, the velocity of the Ryukyu Current is not enough to drag waters above its main core (Wang et al., 2019). However, the Ryukyu Current intensifies along its path, and south of Okinawa, is strong enough to extend its influence to the surface and drag water with it (Wang et al., 2019).

As a geostrophic current belonging to the North Pacific subtropical gyre, the Kuroshio Current intensity is associated with the horizontal gradient of wind stress on the ocean

surface (Hu et al., 2015). Thus, easterlies and westerlies apply respectively a negative and positive wind stress curl over the equatorial Pacific; when negative, it causes an equatorward migration of the North Equatorial Current compensated by the intensification of the poleward Kuroshio Current transport to conserve mass balance, and conversely when positive (Hu et al., 2015; Qiu and Lukas, 1996). This wind stress curl is strongly influenced by the East Asian Monsoon and the El Niño Southern Oscillation. During EASM and La Niña phase, strengthened easterlies induce an increase of the negative wind stress curl, leading to a equatorward migration of the bifurcation and hence an intensification of the Kuroshio Current. Conversely, during EAWM and El Niño phase, the strengthened westerlies and weakened easterlies generate a positive wind stress curl, leading the poleward migration of the bifurcation and hence a weakening of the Kuroshio Current (Hu et al., 2015; Qiu and Lukas, 1996).

3 Materials and methods

The 23 m piston core MD18-3532 (23°28.88'N, 123°5.89'E; water depth: 4325 m) was recovered during the EAGER Cruise of the R/V Marion-Dufresne II in 2018. It was collected at 150 km off the coast of Taiwan, in an intra-slope basin of the Ryukyu arc accretionary wedge and out of the present-day mainstream of the Kuroshio Current (Fig. 1a). It is composed of dark grey clay with no evidence of turbiditic sediment sequences or large mass transported deposits, neither at the naked eye lithology observation, nor on general geometry on seismic profiles (N. Babonneau and G. Ratzov, unpublished data). Few millimetre-thick silt/fine sand layers concentrated in the uppermost 3 m of the core are found, related to the deposition of the queue of fine-grained turbidites derived from turbidite flows thick enough to surmount the topographic barrier and reach East Nanao Basin. Volcanic glass has been observed under

binocular microscope in the > 150 μm size fraction at 165.5 cm depth. No tephra layers can be found at the naked eye inspection.

The age model was built using 13 radiocarbon dates (Table 1) on mixed planktonic foraminifera measured at Alfred-Wegener Institute (Bremerhaven, Germany), using a MICADAS-Accelerator Mass Spectrometry (AMS) and at Laboratoire des Sciences du Climat et de l'Environnement (Saclay, France) using the ECHOMICADAS-AMS facilities. They were converted to calendar ages using Oxcal software version 4.4.4 (Ramsey, 2008) and the Marine20 calibration curve (Heaton et al., 2020). A local correction of the reservoir age of 86 (± 40) years was applied (Dezileau et al., 2016). The volcanic glass shards at 165.5 cm corresponding to the 7300-year-old Kikai-Akahoya (K₁) eruption (Matsu'ura et al., 2021) confirms the age model (Fig. 2).

The sediment core was scanned at 1 cm resolution using an AVAATECH XRF core scanner at IFREMER laboratory "Geo-Ocean" (Plouzané, France) to determine the semi-quantitative elemental composition of the sediment in counts per second (Richter et al., 2006). The $\ln(\text{Br}/\text{Al})$ ratio is commonly used to qualitatively reconstruct the relative abundance of marine organic matter and to differentiate it from terrestrial organic matter, since Br is particularly abundant in the marine realm due to the synthesis of organic bromine-laden compounds by bacteria and microalgae (Channell et al., 2019; Harvey, 1980; Hillenbrand et al., 2021; Mayer et al., 2007; Nieto-Moreno et al., 2011; Ziegler et al., 2008). $\ln(\text{Ti}/\text{Al})$ and $\ln(\text{Fe}/\text{Al})$ can be used to identify the contribution of secondary terrestrial sources of sediments by highlighting their difference in composition of terrigenous elements with the main source, such as aeolian dust supplies in an environment dominated by fluvial inputs (Calvert and Pedersen, 2007; Croudace and Rothwell, 2015; Govin et al., 2012; Martinez-Ruiz

et al., 2015). The XRF ratios were smoothed by a 30-point moving average using XLSTAT software (Addinsoft, 2016).

One-cm thick samples were retrieved from the core approximately every 10 centimetres ($n = 264$), corresponding to an average resolution of 100 years. Three-gr subsamples were used for geochemical analysis and the rest was sieved at $63 \mu\text{m}$ to separate the silt-clay from the sand fraction. Carbon and nitrogen isotopic ($\delta^{15}\text{N}_{\text{sed}}$, $\delta^{13}\text{C}_{\text{org}}$) analyses, as well as measurements of total carbon (TC), total nitrogen (TN) and total organic carbon (TOC) were carried out on those samples. $\delta^{15}\text{N}_{\text{sed}}$, $\delta^{13}\text{C}_{\text{org}}$, TC and TN were analysed on freeze-dried, grounded, and weighed samples at CEFREM laboratory (University of Perpignan, France). $\delta^{15}\text{N}_{\text{sed}}$, $\delta^{13}\text{C}_{\text{org}}$ subsamples were decarbonated using repeated additions of 2 mol.L^{-1} of concentrated hydrochloric acid (HCL) until no effervescence was observed. Isotopic values were measured with a Eurovector 3000 elemental analyser coupled to a GVI-Isoprime mass spectrometer (EA-IRMS). Values are expressed in per mil (‰) relative to the Vienna Pee Dee Belemnite standard (V-PDB) for $\delta^{13}\text{C}_{\text{org}}$ and AIR for $\delta^{15}\text{N}_{\text{sed}}$. All samples were measured at least in duplicate at CEFREM laboratory (University of Perpignan, France). For each series of measurements, High Organic (HO) sediment B2151 and Low Organic (LO) sediment B2153 certified standards were analyzed at the beginning and end of the series. Standard values and errors, as well as the analytical precision and accuracy are reported in Table S1.

TC and TN values were measured on a CHN Elementar at CEFREM laboratory (University of Perpignan, France) and values are expressed in percentage of dry weight (%). TOC was calculated by dividing (i) the mass of absolute C by (ii) the total mass of the sample multiplied by 100. TOC and TN can originate from primary productivity and/or continental input (Hilton et al., 2010; Kao et al., 2014), and they are often used to reconstruct changes in

primary productivity (Meyers, 1997; Stein, 1991). Here, TOC has been compared to Br/Al to distinguish marine organic matter from terrestrial input, and a marine vs. continental $\delta^{13}\text{C}_{\text{org}}$ mixing model has been performed in order to estimate the terrestrial contribution (F_{terr} $\delta^{13}\text{C}_{\text{org}}$) to the organic C accumulation and $\delta^{13}\text{C}_{\text{org}}$ signature. The equation used take the form : $F_{\text{terr}} = (X - X_{\text{M}}) / (X_{\text{T}} - X_{\text{M}})$, with X the $\delta^{13}\text{C}_{\text{org}}$ of the sample, X_{M} the marine $\delta^{13}\text{C}_{\text{org}}$ end-member and X_{T} the terrestrial $\delta^{13}\text{C}_{\text{org}}$ end-member (Kandasamy et al., 2018). For this purpose, the $\delta^{13}\text{C}_{\text{org}}$ terrestrial end-member has been estimated at -22.8‰ and the marine end-member at -20.0‰ (Goericke and Fry, 1994; Kao et al., 2003).

The clay minerals were analysed using the XRD F. Analytical X'Pert PRO at the Centre Européen de Recherches Préhistoriques (Tautavel, France). The analyses were conducted on the 2 μm fraction of 65 evenly distributed samples after decarbonation and oxygenated water degradation of organic matter. The identification and semi-quantification of the different clays was done based on the position and intensity of peaks. Illite and chlorite were analysed based on their main peaks at 14 and 10 Å respectively. Kaolinite was measured based on the ratio between the intensity of the shoulder at 3.5 Å and the intensity of the (002) chlorite peak at 5 Å. The percentages of each clay mineral were determined with respect to the abundance of all detected minerals including clay, quartz, and feldspars peaks at 4.26 and, 3.24-3.18 Å respectively. Illite crystallinity has been calculated as the full width at half maximum of the main illite peak. It can be used to determine the degree of chemical (high values) or physical (low values) alteration of a rock (Li et al., 2012) or as an index of provenance in the case where the source is partly composed of metamorphic rocks (Jaboyedoff et al., 2001; Verdel et al., 2012).

4 Results

4.1 Age model and sedimentation rate

The age model indicates that the core MD18-3532 covers the last 26 kyr (Fig. 2, Table 1). Significant variations in sedimentation rate can be observed and coincide with the depths at which radiocarbon measurements were measured, indicating they are artefacts generated by the calculation model that has been run using only the dated points (Fig. 2). Two periods can be nonetheless highlighted: a “high” sedimentation rate period of 177 cm kyr^{-1} from $13.3 (\pm 0.5)$ to $24.8 (\pm 0.6)$ ka, and a “low” sedimentation rate period of 38 cm kyr^{-1} from $3.5 (\pm 0.3)$ to $13.3 (\pm 2.5)$ ka (Fig. 2 and 3a). Although the exact timing of the transition, 13.3 ± 2.5 (0.5) ka toward the younger (older) date, has a large error, the transition between these two periods takes place during BA.

4.2 Illite crystallinity, clay minerals abundance and grain size

The clay minerals are composed of illite, chlorite and kaolinite (Table 2) and variations are not substantial throughout the core, although higher percentages of illite and chlorite are observed in the Holocene ($11.7 - 0.0$ ka) (Walker et al., 2009) compared to MIS 2, due to the decrease in kaolinite (Fig. 3b). Same as clay minerals, illite crystallinity remain relatively constant throughout the core (Table 2; Fig. 3c). The weight percentage of the $< 63 \mu\text{m}$ fraction ranges from 81.0 to 99.9 with an average of $99.0 (\pm 4.0)$ and, despite some fluctuations, remains stable throughout the core (Fig. 3d).

4.3 X-ray fluorescence (XRF)

$\text{Ln}(\text{Br}/\text{Al})$ values range from -3.70 to -0.46 with an average of $-2.67 (\pm 0.72)$, $\text{Ln}(\text{Fe}/\text{Al})$ range from 2.87 to 4.31 with an average of $3.27 (\pm 0.34)$ and $\text{Ln}(\text{Ti}/\text{Al})$ range from 0.61 to 1.48 with an average of $0.88 (\pm 0.25)$ (Fig. 3e). These three XRF ratios show a similar trend with a

gradual increase during the pre-LGM and LGM with a maximum reached during the Late Glacial (LG; 19.0 – 18.0 ka) and HS1, before beginning to decrease at the end of HS1, from 16 to 7 ka. After 7 ka, the three ratios start to rise again (Fig. 3e). A similar evolution of the trend can also be stated by Spearman correlation. Both terrigenous $\ln(\text{Fe}/\text{Al}, \text{Ti}/\text{Al})$ ratios show a very strong correlation with each other ($r = 0.91$, $p\text{-value} < 0.001$) and a moderate correlation rate with $\ln(\text{Br}/\text{Al})$ ($r = 0.64 - 0.65$, $p\text{-value} < 0.001$) (Table S2). The Spearman correlation coefficient with $\ln(\text{Br}/\text{Al})$ increases after smoothing the data using a 30-order moving average ($r = 0.74$, $p\text{-value} < 0.001$) (Table S3).

4.4 Isotopic geochemistry

$\delta^{15}\text{N}_{\text{sed}}$ values range from -1.6 to 7.4‰ with an average of 3.1‰ (± 3.2) (Fig. 3f). They show relatively high values during the pre-LGM before abruptly decreasing at the beginning of LGM. Then, they observe a sharp decrease to much lower values until the mid-BA, with mean values from LGM to 13.6 ka. After the mid-BA, the $\delta^{15}\text{N}_{\text{sed}}$ rises steeply and stabilizes on a plateau from Younger Dryas (12.9 – 11.7 ka) (Clark et al., 2012) until the Holocene (Fig. 3f).

$\delta^{13}\text{C}_{\text{org}}$ values range from -22.5 to -19.0‰ with an average of -21.3‰ (± 1.1) (Fig. 3g). The record shows high values during the pre-LGM then a decrease during LGM, before starting to increase again during LG to reach a maximum during mid-HS1, around 17.5 – 16 ka. From 16 ka, $\delta^{13}\text{C}_{\text{org}}$ values start to decrease progressively to reach a minimum plateau after 8 ka (Fig. 3g). The marine vs. continental $\delta^{13}\text{C}_{\text{org}}$ mixing model values show that the contribution of marine organic carbon is highest during HS1 and pre-LGM. They show a more moderate marine contribution during LGM, LG and BA, and an increase of the terrestrial contribution since the end of HS1 to a maximum during the Holocene (Fig. 3h).

4.5 Organic geochemistry

TOC values range from 0.33 to 0.79% with an average of 0.57% (± 0.17) (Fig. 3i). They show an increase from the pre-LGM to HS1, then a decrease from Bølling–Allerød (BA; 14.7 – 12.9) (Clark et al., 2012) until reaching a minimum during the Holocene (Fig. 3i). TN values range from 0.05 to 0.14% with an average of 0.09% (± 0.03) (Fig. 3j). They show an increase from the pre-LGM to LG, then a decrease until the mid-BA, before rising slightly during the Holocene (Fig. 3j).

5 Discussion

5.1 Origin of sediments in core MD18-3532

Clay minerals relative abundance show that the sediments of core MD18-3532 are dominated by illite and chlorite with traces of kaolinites (Fig. 4e). In the South and East China Seas, clay mineral assemblages are commonly used to reconstruct the source of terrigenous sediments (Diekmann et al., 2008; Dou et al., 2010; Liu et al., 2016, 2010; Steinke et al., 2008; Wan et al., 2010). Previous studies have evidenced that in the region, three sources are characterized by dominance of illite and chlorite with rare presence of kaolinite: (i) the Yangtze River and the East China Sea shelf, (ii) the Taiwan island and (iii) the Chinese Loess Plateau (Diekmann et al., 2008; M. He et al., 2013; Li et al., 2012; Nayak et al., 2021; Wan et al., 2007; Zhao et al., 2017).

In Taiwan island, the dominance of illite and chlorite is related to intense physical erosion and the rapid transfer of eroded sediments to the ocean, which prevents the chemical erosion necessary for the formation of kaolinite (Chamley, 1989; Li et al., 2012). In addition, the Central Taiwan Range is composed of polymetamorphic rocks with an abundance of slates and schists that generate illite and chlorite (Ho, 1986; Li et al., 2012; Nayak et al.,

2022). Thus, kaolinite is only a minor mineral of Taiwan, mainly found in Hengchun Peninsula and Kenting Plateau, the southern tip of the Taiwan Central Range and its southern submarine plateau, and Tainan Shelf, on the SW coast, with an average concentration of 10% (Nayak et al., 2021).

The Yangtze River originates in the eastern part of the Tibetan plateau, whose high elevation (>6000 m) leads to increased erosion and cold climate, resulting in a significant formation of illite. The bedrock in the upper Yangtze watershed includes intermediate-acid igneous rocks and basic basalts which favor the formation of illite and chlorite (M. He et al., 2013). In contrast, indexes of chemical alteration, erosion and crystallinity of illite indicate an increase of chemical weathering in the middle and downstream sections of the watershed relative to upstream (M. He et al., 2013). It is marked by an enrichment of kaolinite due to the chemical erosion of granites containing potassium feldspars and muscovite which are sources of kaolinite under chemical weathering conditions (M. He et al., 2013). Thus, Yangtze transported particulate matter deposits mostly illite and chlorite on the East China Sea shelf, with kaolinite present up to 10% on average (M. He et al., 2013; Liu et al., 2006).

The Chinese Loess Plateau clay mineral assemblage is dominated by illite and chlorite with little amount of kaolinite (6 – 10%) (Wan et al., 2007; Zhao et al., 2017). Illite and chlorite originate from the erosion of very low- to low-grade metamorphic rocks eroded by EAWM winds from northern region of the Tibetan Plateau (Ji et al., 1999), while the prevailing aridity and low temperatures in the loess region, particularly during glacial periods, limit the chemical weathering that would lead to kaolinite formation (Chamley, 1989; Maher, 2016).

Core MD18-3532 clay minerals abundance could therefore potentially be related to (i) erosion of Taiwan massifs, (ii) sediment transport from the Yangtze River, especially during low sea level periods, and (iii) airborne transport of loess sediments mainly during glacial periods. The Yangtze River source (ii) might be particularly important if we consider a weakening of the Kuroshio Current through the Okinawa Trough, and the potential establishment of a counter-current in the Okinawa Trough similar to the modern Zhejiang-Fujian Coastal Current. This latter can originate by an enhanced EAWM, transporting sediments southward. The Yangtze River contribution to the sedimentation of the southern Okinawa Trough during the deglaciation is supported by the mineralogical composition of sediment at the ODP 1202B site (Diekmann et al., 2008) (Fig. 1a). The third source would have been particularly intense during LGM and HS1 due to intensified EAWM (E. Huang et al., 2011; Sun et al., 2012; Yang et al., 2020). It was caused by the increase of the zonal land-sea thermal contrast between Eurasia and North Pacific by the cooling of the North Hemisphere, resulting in the intensification of the Siberian High over Eurasia (Kutzbach, 1993; Sun et al., 2012) and Aleutian Low over the western North Pacific (McGee et al., 2018; Yanase and Abe-Ouchi, 2007). During HS1, the Atlantic Meridional Overturning Circulation weakening in the North Atlantic, combined with the setting of El Niño-like state in the equatorial Pacific (Clement et al., 1999; Merkel et al., 2010; Timmermann et al., 2007), would have resulted in an even stronger intensification of EAWM than during LGM as evidenced by the maximum observed in the Gulang Loess mean grain size (Fig. 4b) (E. Huang et al., 2011; Sun et al., 2012; Yang et al., 2020).

In order to disentangle the potential sediment sources we compared measured illite crystallinity values from core MD18-3532 with those measured in previous studies in sediments from Taiwan rivers, Chinese Loess Plateau, the Yangtze River and the East China

Sea shelf. Illite crystallinity measured present much lower values than those of loess (C. Huang et al., 2011; Ji et al., 1999), East China Sea shelf and the Yangtze River (M. He et al., 2013) (Fig. 5). These values are characteristic of Fe-Mg rich un-weathered illite and of physically eroded greenschists typical of the Central Range of Taiwan (Li et al., 2012; Nayak et al., 2021) and the stability of these values over the past 26 kyr suggest a steady sediment source (Fig. 4f). The source of the kaolinite is more difficult to ascertain, but given the clearly Taiwanese signal of illite crystallinity, we suggest that the kaolinite originates from the Hengshun Peninsula, southern Taiwan, and remobilization of Keating Plateau sediments by erosion caused by the Kuroshio Current (Das et al., 2021).

However, although Taiwan appears to be the main and constant source of sediment, secondary sources bringing insufficient amounts of sediment to influence the clay assemblage may exist. Using $\ln(\text{Fe}/\text{Al})$ and $\ln(\text{Ti}/\text{Al})$, we observed an increase in these elemental ratios from LGM to HS1 before starting to decrease during BA that might indicate supply of terrigenous material from another source than Taiwan (Fig. 4g). As $\ln(\text{Ti}/\text{Al})$ and $\ln(\text{Fe}/\text{Al})$ show a very strong Spearman correlation degree ($r = 0.91$; Table S2), it suggests that $\ln(\text{Fe}/\text{Al})$ is not affected by redox mechanisms and that both ratios reflect terrestrial inputs (Croudace and Rothwell, 2015). Changes in these elemental ratios might be related to grain size sorting due to the presence of Ti- and Fe-bearing heavy minerals in the coarse fraction (Croudace and Rothwell, 2015; Zhao et al., 2011), but low abundance and small variation in the sandy fraction suggest that grain size doesn't have any effect on these elemental ratios (Fig. 3d). The $\ln(\text{Ti}/\text{Al})$ and $\ln(\text{Fe}/\text{Al})$ trends are more similar to the evolution of the EAWM winds intensity as registered in the Gulang Loess mean grain size (Sun et al., 2012) and dust mass accumulation rate in core MD06-3047, collected east off Philippines (Xu et al., 2015) than to sea level changes (Lambeck et al., 2014) (Fig. 4b). This suggests dust-

borne Fe and Ti inputs by enhanced EAWM rather than related to the emergence of the East China Sea shelf and southeastward migration of the Yangtze River mouth.

5.2 Changes in the Kuroshio Current pathway

Given that Taiwan has been established as the major and constant source of sediment, we investigate hypotheses that could explain the high sedimentation rate observed from LGM to BA (Fig. 4d). From the LGM to HS1, the weakening of the easterly trade winds due to an enhanced EAWM (Cheng et al., 2016; Steinke et al., 2010; Sun et al., 2012), El Niño-like conditions (Clement et al., 1999b; Ford et al., 2015; Koutavas et al., 2002; Yamamoto, 2009) and weakened Walker Circulation (Hollstein et al., 2018; Tian and Jiang, 2020) led to the decrease of the positive wind stress curl over the equatorial North Pacific (Hu et al., 2015). This would have caused the northward migration of the North Equatorial Current bifurcation resulting in the weakening of the Kuroshio Current (Hu et al., 2015; Qu and Lukas, 2003; Zou et al., 2021). Therefore, Kuroshio Current's decline could have caused a reduction of the "barrier effect", allowing surface sediment plumes to spread eastwards, toward the study area.

On the other hand, at least partial deflection of the Kuroshio Current along the eastern edge of the Ryukyu Arc might also have transported eroded sediments from Taiwan to the study site. This deflection could have been caused by the ~130 m drop in sea level during the LGM (Lambeck et al., 2014) decreasing the water depth in the Yonaguni depression. This would have caused an increase in the intermediate water volume diverted eastwards, strengthening the Ryukyu Current and ultimately dragging the surface water to form an eastern branch of the Kuroshio Current (Fig. 6).

Both hypotheses are consistent with an increase in the sedimentation rate from LGM to BA (Fig. 4d). Previous publications observed an intensification of the Kuroshio Current in the Okinawa Trough during BA (Li et al., 2020, 2019; Lim et al., 2017) (Fig. 7d and 7e) that could have been induced by a renewed efficiency of the “water barrier” effect. On the other hand, the sea level rise from – 100 to – 60 m during BA (Lambeck et al., 2014) (Fig. 7c) might be at the origin of a decrease in the Ryukyu Current intensity by reducing the intermediate water volume diverted eastward and increasing it in the Yonaguni Depression. This would have resulted in the collapse of the Kuroshio Current eastern branch and intensification of the Kuroshio Current in the Okinawa Trough as observed in the increase of sea surface temperatures (Li et al., 2020; Sun et al., 2005) (Fig. 7d), deepening of the thermocline (Li et al., 2020) (Fig. 7e) and in the relative contribution of detrital ferrimagnetic minerals to bulk magnetic properties (Li et al., 2019).

From 22.5 – 13.6 ka, the high sedimentation rate is concomitant with $\delta^{15}\text{N}_{\text{sed}}$ values averaging 2.1‰ (± 1.3) (Fig. 7g). These low values might be attributed to three mechanisms: (i) grain size sorting effect (Robinson et al., 2012; Schubert and Calvert, 2001), (ii) continental influence due to the main dominance of illite in Taiwanese clay mineral assemblages (Robinson et al., 2012) or (iii) nitrogen fixation by cyanobacteria (Galbraith et al., 2008; Kim et al., 2017). The high abundance and the small variation of the < 63 μm fraction (Fig. 3d) suggest that grain size sorting (i) does not have any effect on $\delta^{15}\text{N}_{\text{sed}}$ signature. The continental influence (ii) is potentially possible, as it is linked to the presence of NH_4^+ in the interfoliar space of illite clay. However, $\delta^{15}\text{N}_{\text{sed}}$ and TN data show a non-significant Spearman correlation with illite ($p > 0.05$; Table S4), indicating that illite inputs have no influence on $\delta^{15}\text{N}_{\text{sed}}$ or TN values. Furthermore, measurements in rocks from Taiwan show higher $\delta^{15}\text{N}$

values (>3‰) (Owen, 2013; Yui et al., 2009) suggesting that terrestrial input from Taiwan do not influence $\delta^{15}\text{N}_{\text{sed}}$.

Thus, we suggest that the $\delta^{15}\text{N}_{\text{sed}}$ records is mainly controlled by nitrogen fixation. The Kuroshio Current carries abundant *Trichodesmium* spp. cyanobacteria that originate in blooms around the Pacific island along its path (Chen et al., 2008; Shiozaki et al., 2015; Wu et al., 2018). Their abundance decreases with distance from the coast in east Taiwan (Chen et al., 2018) and they generate significant nitrogen fixation in the Kuroshio Current compared to the rest of the Philippine Sea (Liu et al., 1996; Shiozaki et al., 2015) with a specific $\delta^{15}\text{N}$ signature around $-0.9 \pm 1.0\text{‰}$ (Eberl and Carpenter, 2007; Liu et al., 1996; Wada and Hattori, 1976). The observed decrease in $\delta^{15}\text{N}_{\text{sed}}$ during the period of high sedimentation rate (Fig. 7g) might have been caused by the supply of these cyanobacteria over the study area by an eastern branch of the Kuroshio Current, suggesting rather a partial deflection of the Kuroshio Current than a decrease of the “water barrier” effect (Fig. 6). During and after BA, the collapse of the Kuroshio Current eastern branch due to the rise of sea level and the intensification of the Kuroshio Current in the Okinawa Trough induced by enhanced EASM and transition to a La Niña-like state led to the decrease in sedimentation rates and an increase in $\delta^{15}\text{N}_{\text{sed}}$ (Fig. 7c, 7e and 7g).

5.3 Kuroshio and East Asian Winter Monsoon controls on primary productivity

Northeast of Taiwan, south of the Okinawa Trough, present-day measurements in surface sediments under the modern path of the Kuroshio Current observed $\delta^{15}\text{N}_{\text{sed}}$ values greater than 3‰ (Kao et al., 2003). This isotopic signature, close to those of the Taiwanese rocks (Owen, 2013; Yui et al., 2009), indicates that the signal is dominated by terrigenous inputs of nitrogen rather than by cyanobacterial activity despite the presence of

Trichodesmium spp. in the Kuroshio Current above (Jiang et al., 2019; Liu et al., 1996). Therefore, the mere input of cyanobacteria might not be enough to explain the decrease of $\delta^{15}\text{N}_{\text{sed}}$. During LGM and HS1, the strengthened EAWM would have caused an increase in dust-borne Fe inputs as evidenced by $\ln(\text{Fe}/\text{Al})$ (Fig. 7h), soluble iron concentration and dust mass accumulation rate in core MD06-3047 (Xu et al., 2015) (Fig. 7b). In addition a deepening of the mixed layer as observed in the northern South China Sea (Steinke et al., 2010; Zhang et al., 2016) can result in the upwelling of sub surface water. It would have caused a transfer of phosphate and nitrate from the nutrient-rich Kuroshio Current subsurface water (Chen et al., 2017, 2021, 1995) to the surface of these co-limiting nutrients (Fe, P) with consequent intensification of nitrogen fixation by cyanobacterial activity (Held et al., 2020; Lis et al., 2015; Qiu et al., 2021). This hypothesis is supported by the concomitant enhancement of nitrogen fixation in the Okinawa Trough as evidenced by the organic nitrogen $\delta^{15}\text{N}$ ($\delta^{15}\text{N}_{\text{ON}}$) of core MD01-2404 (Zheng et al., 2015) (Fig. 7g). In the East China Sea, the nitrogen fixation is strongly related to the input of *Trichodesmium* spp. by the Kuroshio Current (Jiang et al., 2019; Liu et al., 1996; Zhang et al., 2012). This synchronous evolution (Fig. 7g) suggests that during LGM and HS1, both the remaining and deflected branches would have transported cyanobacteria northern and southern of the Okinawa Trough, and their nitrogen fixation would have been increased by an enhanced EAWM. This observation is consistent with the hypothesis of total or partial deflection from LGM to BA (Fig. 6), and highlights the control exerted by the Kuroshio Current and EAWM on nitrogen fixation in this region.

Enhanced paleoproductivity is also evidenced by the concomitant increase in $\ln(\text{Br}/\text{Al})$, $\delta^{13}\text{C}_{\text{org}}$ and TOC (Fig. 7h – 7j) from LGM to HS1 before decreasing during and after BA. This is consistent with an enhanced EAWM winds intensity and deflection of the Kuroshio Current

from LGM to BA, then a reduction of EAWM winds intensity and the collapse of the Kuroshio Current eastern branch caused by the sea level rise during and after BA (Fig. 7b and 7c). This would have resulted in the weakening of the dust-borne Fe inputs and the shallowing of the mixed layer, and the cessation of N and P supply by the Kuroshio Current subsurface waters. The impact of dust-borne Fe inputs and/or monsoonal upwelling of nutrients from the subsurface on primary productivity during LGM and HS1 is supported by previous studies in the northern South China Sea (J. He et al., 2013; Zhang et al., 2016; Zhou et al., 2016), in the Okinawa Trough (Ruan et al., 2017) and southern Philippine Sea (Xu et al., 2020, 2015), and by a modern study showing that N is the first-order limiting nutrient and P, Fe are second-order co-limiting nutrient in the study area (Browning et al., 2022). Although the impact of Kuroshio Current and EAWM on paleoproductivity can be observed in the Okinawa Trough by the biogenic silica concentration (BSi) in core KX12-3 and $\delta^{15}\text{N}_{\text{ON}}$ in core MD01-2404 (Fig. 8e and 8f), in most of these records their impact is only secondary compared with the emergence of the continental shelf, remobilization/erosion of its sediments, and the migration of river mouths due sea level changes (Chen et al., 2023; Lim et al., 2017; Ruan et al., 2017; Xu et al., 2020) (Fig. 8d, 8g – h and 8j – 8k). East of Taiwan, the limited size of the shelf (Fig. 1a) and the low impact of Taiwanese sediments on primary productivity (Wang et al., 2018) render this influence negligible, explaining the discrepancies observed between paleoproductivity records along the Kuroshio Current south – north transect from the east of the Philippine Sea to the Okinawa Trough (Fig. 8d – 8k).

During HS1, $\delta^{15}\text{N}_{\text{sed}}$ is marked by a significant (p -value < 0.0001; Mann-Whitney U test (Mann and Whitney, 1947)) increase from 1.8‰ (± 1.7) to 2.5‰ (± 1.3) (Fig. 7g) concomitant with the premature decline of TN (Fig. 7k) relative to other paleoproductivity proxies ($\ln(\text{Br}/\text{Al})$, $\delta^{13}\text{C}_{\text{org}}$, TOC) (Fig. 7h – 7j). This might have been caused by the intensification of

water wind stress resulted due to enhanced EAWM that could have limited the development of *Trichodesmium* spp. and their ability to fix atmospheric N (Breitbarth et al., 2007; Chen et al., 2008; Wu et al., 2018). Thus, despite an increase in dust-Fe inputs and summer temperatures above 24°C (Kim et al., 2015) consistent with *Trichodesmium* spp. ecological needs (Breitbarth et al., 2007), cyanobacterial productivity declined, and so did biogenic nitrogen production (7g and 7k).

6 Conclusion

A multi-proxy study of the MD18-3532 core, in the Fvuku accretionary wedge off East Taiwan, has investigated the variability of the Kuroshio Current pathway and paleoproductivity during the last 26 kyr.

High values of sedimentation rate, the distribution of clay minerals, and the low values of $\delta^{15}\text{N}_{\text{sed}}$ from 22.5 to 13.6 ka suggest a partial deflection of the Kuroshio Current along the eastern edge of the Ryukyu Arc during LGM until BA, and hence a transport of (i) Taiwanese suspended material and (ii) *Trichodesmium* spp. cyanobacteria to the coring site. At the same time, high values of $\delta^{13}\text{C}_{\text{org}}$, $\ln(\text{Br}/\text{Al})$, $\ln(\text{Ti}/\text{Al})$, $\ln(\text{Fe}/\text{Al})$, TOC, TN and the low $\delta^{15}\text{N}_{\text{sed}}$ values suggest that EAWM and Kuroshio Current are the main control mechanisms on paleoproductivity in the northwestern Philippine Sea during that time period. Partial deflection of the Kuroshio Current provides nutrient-enriched subsurface waters that upwell toward the oligotrophic surface waters by deepening the mixed layer due to intensified EAWM winds, which also carry dust-borne Fe, thus creating conditions conducive to an increase of primary productivity. After BA, the collapse of the eastern branch of the Kuroshio Current due to sea level rise and the weakening of the EAWM leads to a decrease in the supply of sediment, *Trichodesmium* spp. and nutrients to the eastern edge of the Ryukyu Arc

and a shallowing of the mixed layer, thus reducing primary productivity and sedimentation rates.

Declaration of Competing Interest

The authors declare that they have no known competing financial interests or personal relationships that could have appeared to influence the work reported in this paper.

Acknowledgements

We would like to thank the crew and shipboard scientists of R/V *Marion Dufresne*, during MD214/EAGER cruise, partially funded by the National Energy Program-Phase II (NEPII) project of Ministry of Science and Technology (MOST) of Taiwan and supported by the International Research Project (IRP): From Deep Earth to Extreme Events (D3E) between Centre National de la Recherche Scientifique (CNRS) of France and MOST of Taiwan. We would like to thank Thibaud Saos from the Centre Européen de Recherches Préhistoriques de Tautavel (EPCC), Pierre Giresse and Wolfgang Ludwig from the Centre de Formation et de Recherche sur les Environnements Méditerranéens (CEFREM) for useful help in analyses and discussions. The authors acknowledge the CNRS INSU-SYSTER program for financial support through the ACTEE project, and the comments of two anonymous reviewers and of the editor, that have greatly improved the original manuscript.

Data Availability

The data presented in this study are available in the Pangaea database. Fenies, Pierrick; Bassetti, Maria Angela; Vazquez Riveiros, Natalia; Menniti, Christophe; Frigola, Clément; Babonneau, Nathalie; Ratzov, Gueorgui; Hsu, Shu-Kun; Su, Chih-Chieh (publication year):

XRF, carbon and nitrogen organic and isotopic geochemistry, clay mineral and grain size data from sediment core MD18-3532, eastern Taiwan, over the past 26 kyr. PANGAEA, <https://doi.org/10.1594/PANGAEA.959561>.

CRedit author statement

Fenies, Pierrick: conceptualization, methodology, formal analysis, writing – original draft, visualization; **Bassetti, Maria-Angela:** conceptualization, writing – review & editing, supervision, project administration, funding acquisition; **Vazquez Riveiros, Natalia:** conceptualization, writing – review & editing, supervision, project administration; **Menniti, Christophe:** validation, investigation; **Frigola, Clément:** investigation; **Babonneau, Nathalie:** resources, writing – review & editing, funding acquisition; **Ratzov, Gueorgui:** resources, writing – review & editing, funding acquisition; **Hsu, Shu-Kun:** resources, writing – review & editing, funding acquisition; **Su, Chih-Chieh:** resources, writing – review & editing, funding acquisition.

7 Figures

Table 1: AMS ^{14}C ages and instrumental error, calendar ages and error ($\pm 2\sigma$) for sediment core MD18-3532. Radiocarbon measurements were performed on the following taxa: *Globigerinoides*, *Neogloboquadrina*, *Pulleniatina obliquiloculata* and *Globigerinita glutinata*.

Depth (cm)	AMS ^{14}C age (y)	Error (y)	Calibrated Age (ka)	Error ($\pm 2\sigma$, ka)
15.5	3814	83	3.5	0.3
72.5	5284	67	5.4	0.2
233.5	8640	80	9.0	0.3

375.5	12066	47	13.3	0.2
550.5	12484	47	13.8	0.2
870.5	14442	53	16.6	0.3
1000.5	15235	127	17.5	0.4
1279.5	16385	158	18.8	0.4
1554.5	17815	202	20.5	0.5
1842.5	19482	239	22.4	0.4
1961.5	19687	240	22.9	0.5
2079.5	21241	277	24.3	0.6
2157.5	21562	286	24.8	0.6

Table 2: Average, standard deviation ($\pm 2\sigma$), maximum and minimum clay mineral abundance (%) and illite crystallinity values ($\Delta^\circ 2\theta$) of core MD18-3532.

Clay mineral	Mean abundance	Standard Deviation	Maximum abundance	Minimum abundance
Illite	43	6	37	51
Chlorite	18	6	22	36
Kaolinite	19	6	0	18
Illite crystallinity	0.12	0.06	0.08	0.18

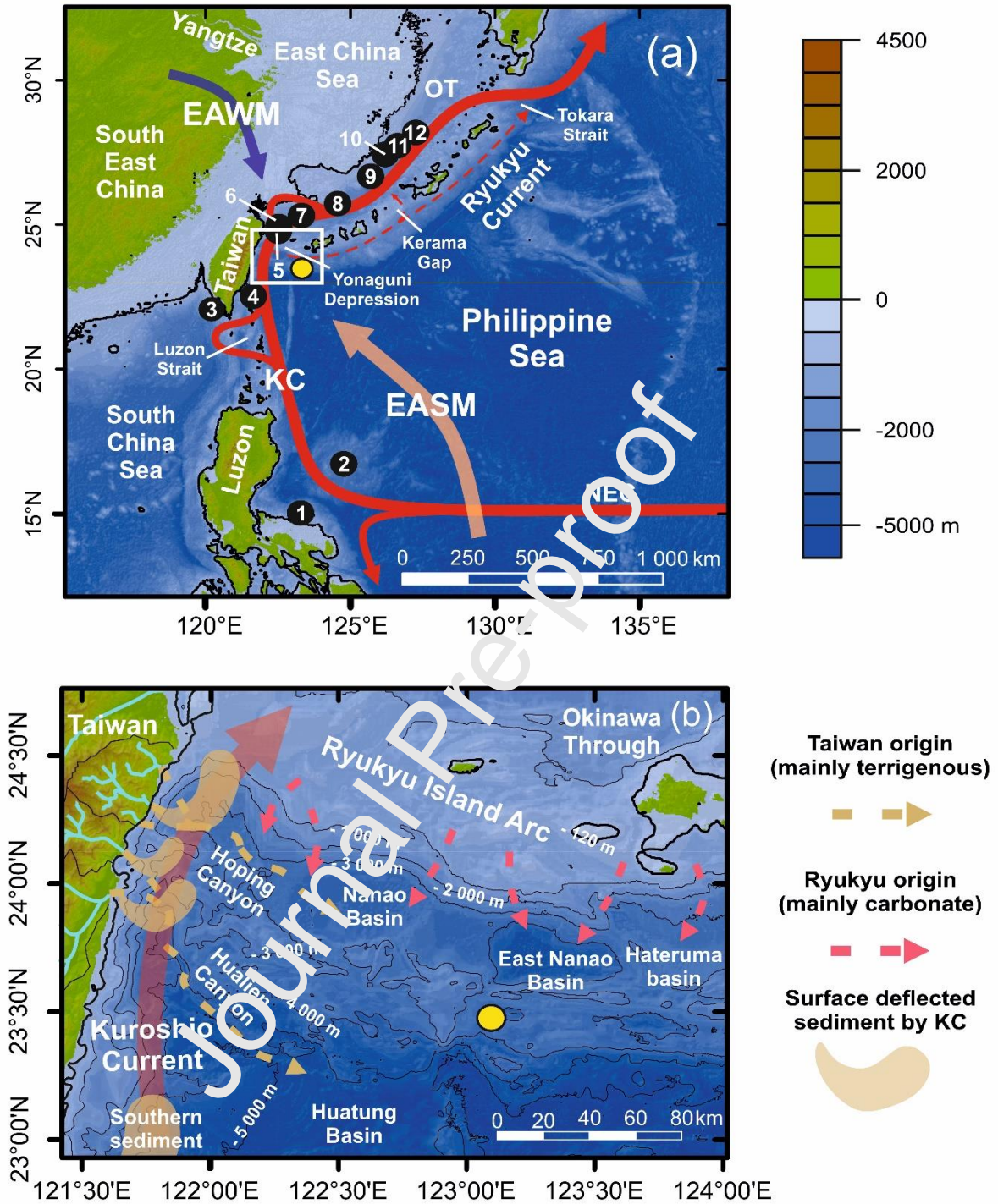


Figure 1: Maps showing (a) the modern Kuroshio Current pathway East of Taiwan and the monsoon pattern in the northwestern Philippine Sea and (b) the bathymetry of the study area and the different modern sedimentary sources. The yellow circle marks the position of the core MD18-3532. The black circles indicate the positions of the cores MD06-3052 (1),

MD06-3047 (2), MD10-3291 (3), OR1715-21 (4), MD05-2908 (5), ODP 1202-B (6), core 255 (7), RN93-PC6 (8), MD01-2404 (9), KX12-3 (10), M063-05 (11) and A7 (12). The 130 m isobath is marked by a thicker black line and shows the emerged area at the last glacial maximum. The white rectangle shows the position of the more detailed box Fig. 1b. The solid red arrow show the Kuroshio Current (KC) pathway, the dotted red arrow show the Ryukyu Current pathway, the blue arrow indicate the East Asian Winter Monsoon (EAWM), the orange arrow indicate the East Asian Summer Monsoon (EASM). NEC: North Equatorial Current, OT: Okinawa Through.

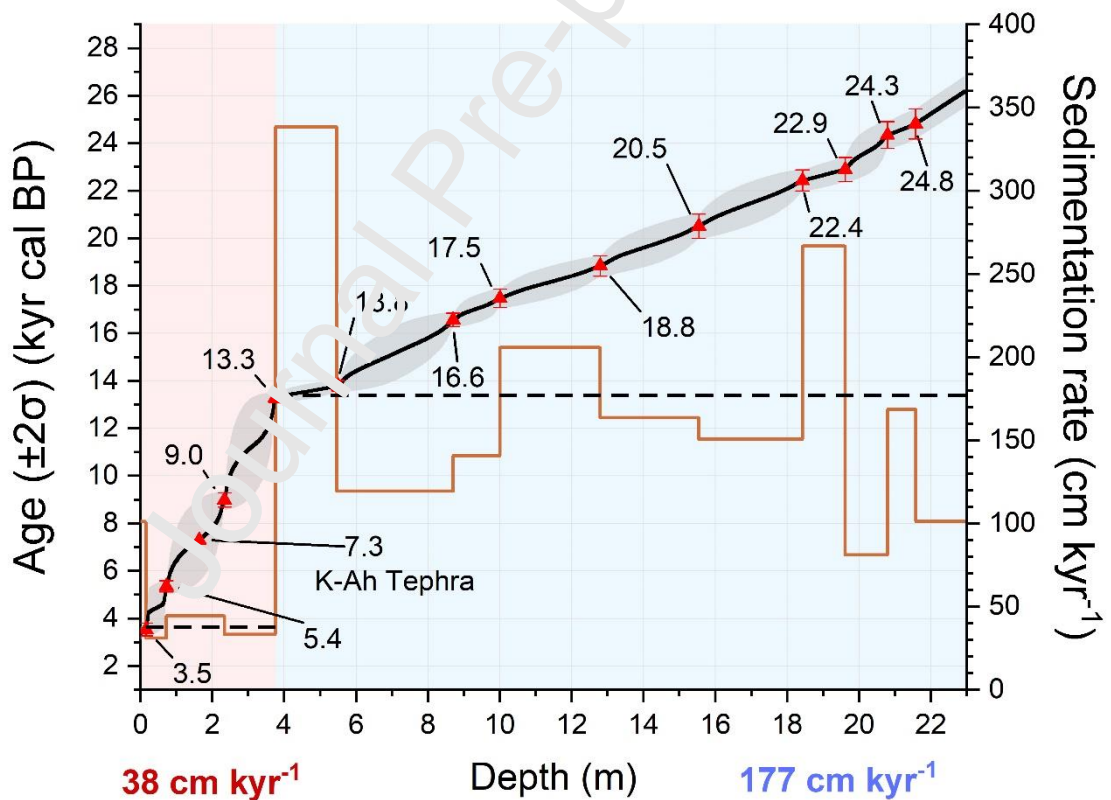


Figure 2: Age model and sedimentation rate of core MD18-3532. All dates are given in calibrated radiocarbon kyr ($\pm 2\sigma$). The black curve is the Oxcal age model and the grey area shows the age model error at 2σ . The dotted lines show the average sedimentation rates

from 3.5 to 13.3 kyr (38 cm kyr^{-1}) and from 13.3 to 24.8 kyr (177 cm kyr^{-1}). The brown curve shows the evolution of the sedimentation rate in cm.kyr^{-1} .

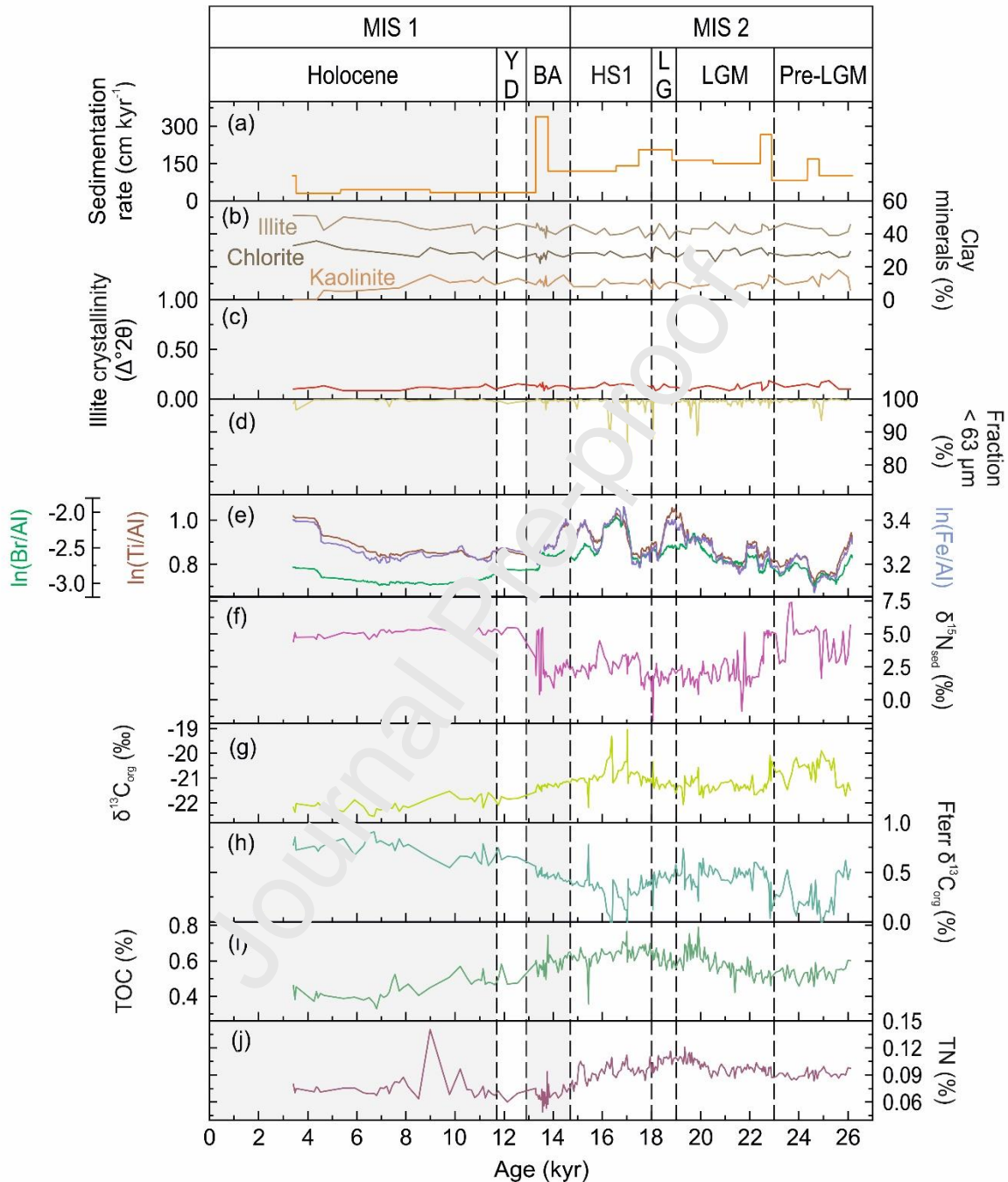


Figure 3: Results of sedimentological and geochemical measurements on core MD18-3532:

(a) sedimentation rate (cm kyr^{-1}), (b) clay minerals (%), (c) illite crystallinity values ($\Delta^\circ 2\theta$), (d) sediment fraction smaller than $63 \mu\text{m}$ (%), (e) elemental ratios $\ln(\text{Br}/\text{Al})$, $\ln(\text{Ti}/\text{Al})$ and

ln(Fe/Al), (f) $\delta^{15}\text{N}_{\text{sed}}$ (‰), (g) $\delta^{13}\text{C}_{\text{org}}$ (‰), (h) terrigenous contribution of terrestrial organic matter to $\delta^{13}\text{C}_{\text{org}}$ (%) estimated from the marine vs. continental $\delta^{13}\text{C}_{\text{org}}$ mixing model, (i) Total Organic Carbon (TOC; %), Total Nitrogen (TN; %). The division of the time scale is first done on the scale of marine isotope stages (MIS), and then on the scale of late Quaternary millennium-scale changes with: Pre-Last Glacial Maximum (Pre-LGM), Last Glacial Maximum (LGM), Late Glacial (LG), Heinrich Stadial 1 (HS1), Bølling-Allerød (BA), Younger Dryas (YD) and Holocene. Dotted lines show the limits of each millennium-scale changes and grey areas are for warming period.

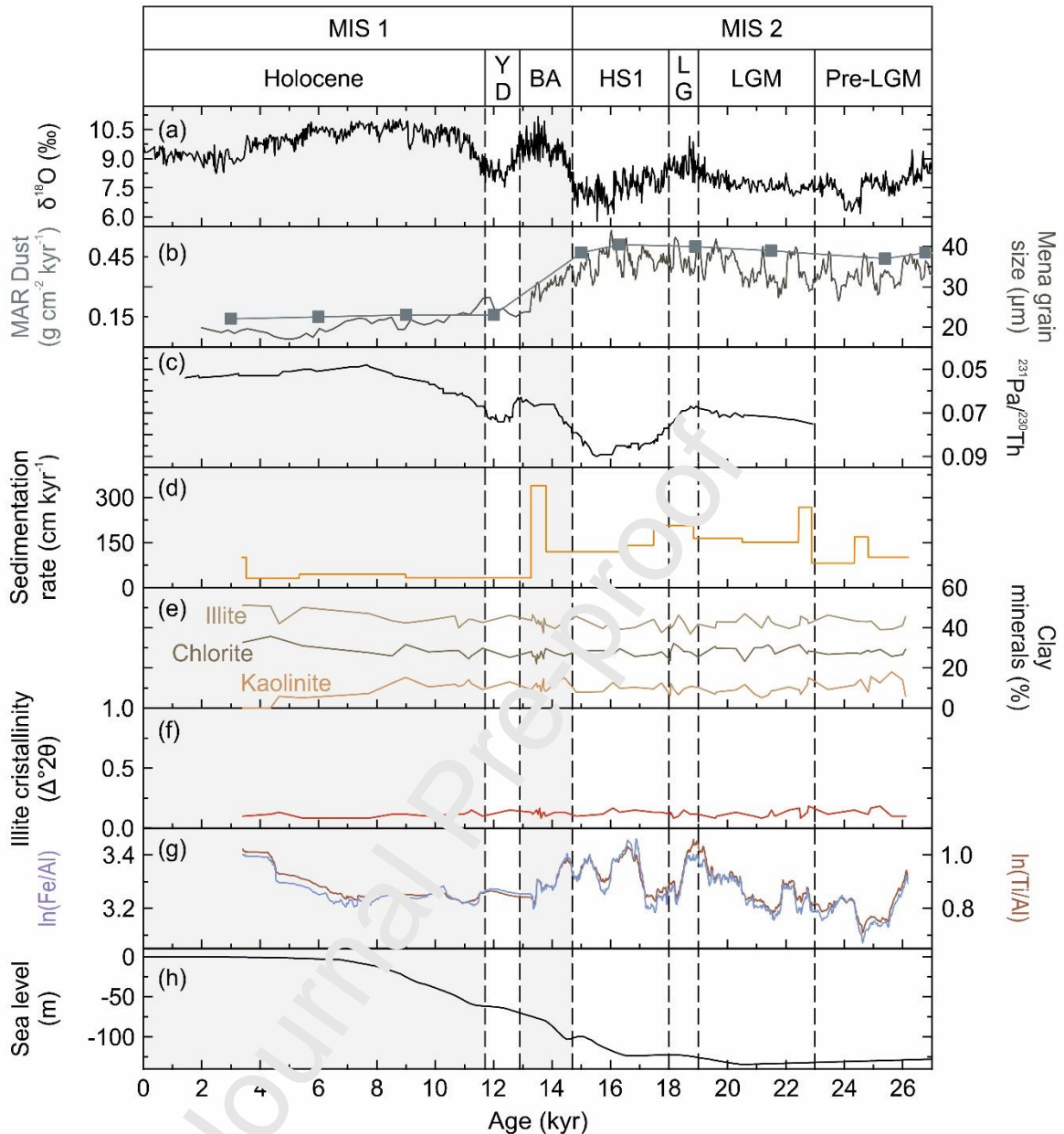


Figure 4: Evolution of terrigenous input and their origin: (a) the $\delta^{18}\text{O}$ of speleothem from Hulu and Dongge caves represents the evolution of the East Asian Summer Monsoon (Cheng et al., 2016), (b) Gulang Loess mean grain size (μm) (Sun et al., 2012) shows changes in the intensity of the East Asian Winter Monsoon (EAWM) and dust mass accumulation rate (MAR) shows the variability of the amount of dust ($\text{g cm}^{-2} \text{ kyr}^{-1}$) brought to the ocean from the Chinese Loess Plateau by the EAWM winds in core MD06-3047, east of the Philippines (Xu et

al., 2015; Fig. 1a), (c) $^{231}\text{Pa}/^{230}\text{Th}$ shows changes in the intensity of the Atlantic Meridional Overturning Circulation (McManus et al., 2004); (d) to (g) data are from core MD18-3532: (d) sedimentation rate (cm kyr^{-1}), (e) percentage of clay minerals (%), (f) illite crystallinity values ($\Delta^{\circ}2\theta$), (g) elemental ratios $\ln(\text{Fe}/\text{Al})$ and $\ln(\text{Ti}/\text{Al})$; (h) relative sea level (Lambeck et al., 2014). The division of the time scale is first done on the scale of marine isotope stages (MIS), and then on the scale of late Quaternary millennium-scale changes with: Pre-Last Glacial Maximum (Pre-LGM), Last Glacial Maximum (LGM), Late Glacial (LG), Heinrich Stadial 1 (HS1), Bølling-Allerød (BA), Younger Dryas (YD) and Holocene. Dotted lines show the limits of each millennium-scale changes and grey areas are for warming period.

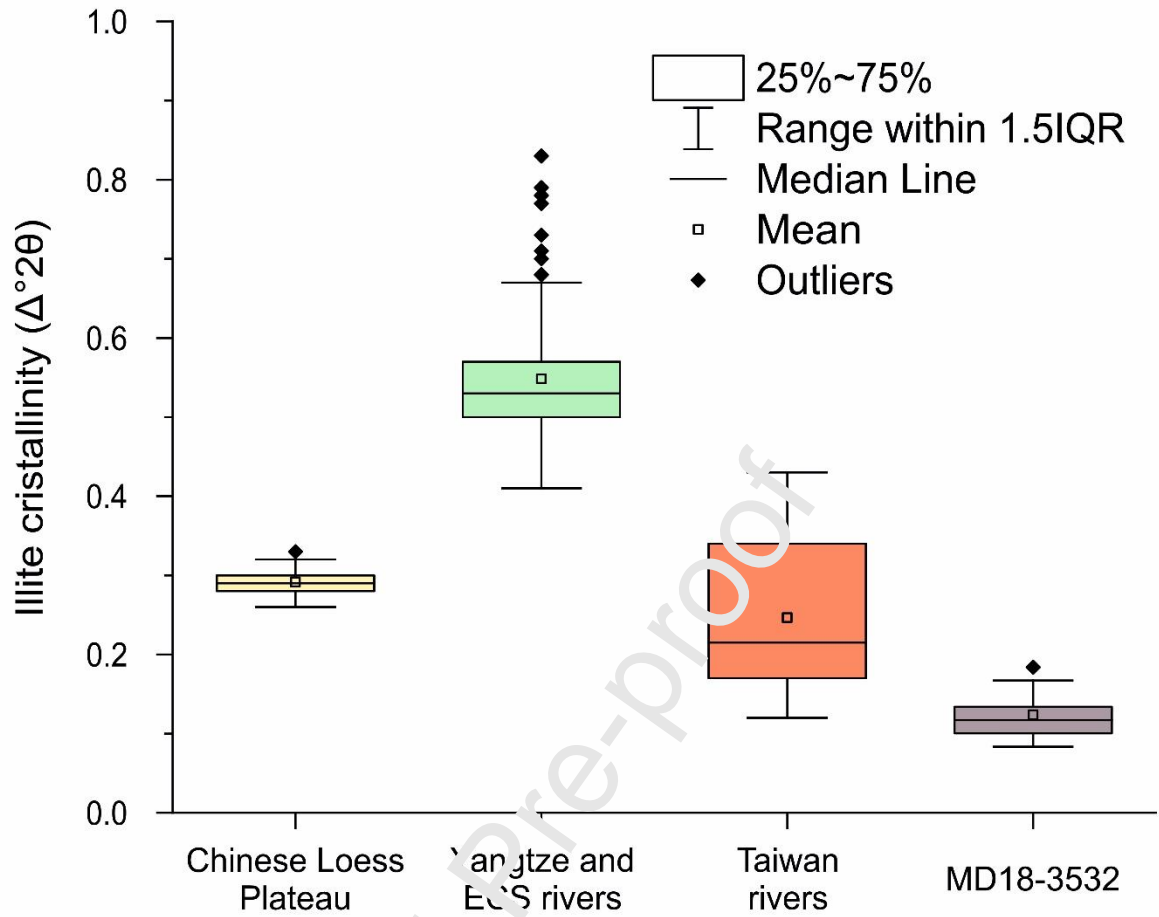


Figure 5: Illite crystallinity values ($\Delta^{\circ}2\theta$) in sediments from the Chinese Loess Plateau (C. Huang et al., 2011; Ji et al., 1992), the Yangtze River and East China Sea shelf (Zhao et al., 2018), Taiwan rivers (Li et al., 2012; Nayak et al., 2021) and MD18-3532 (this study).

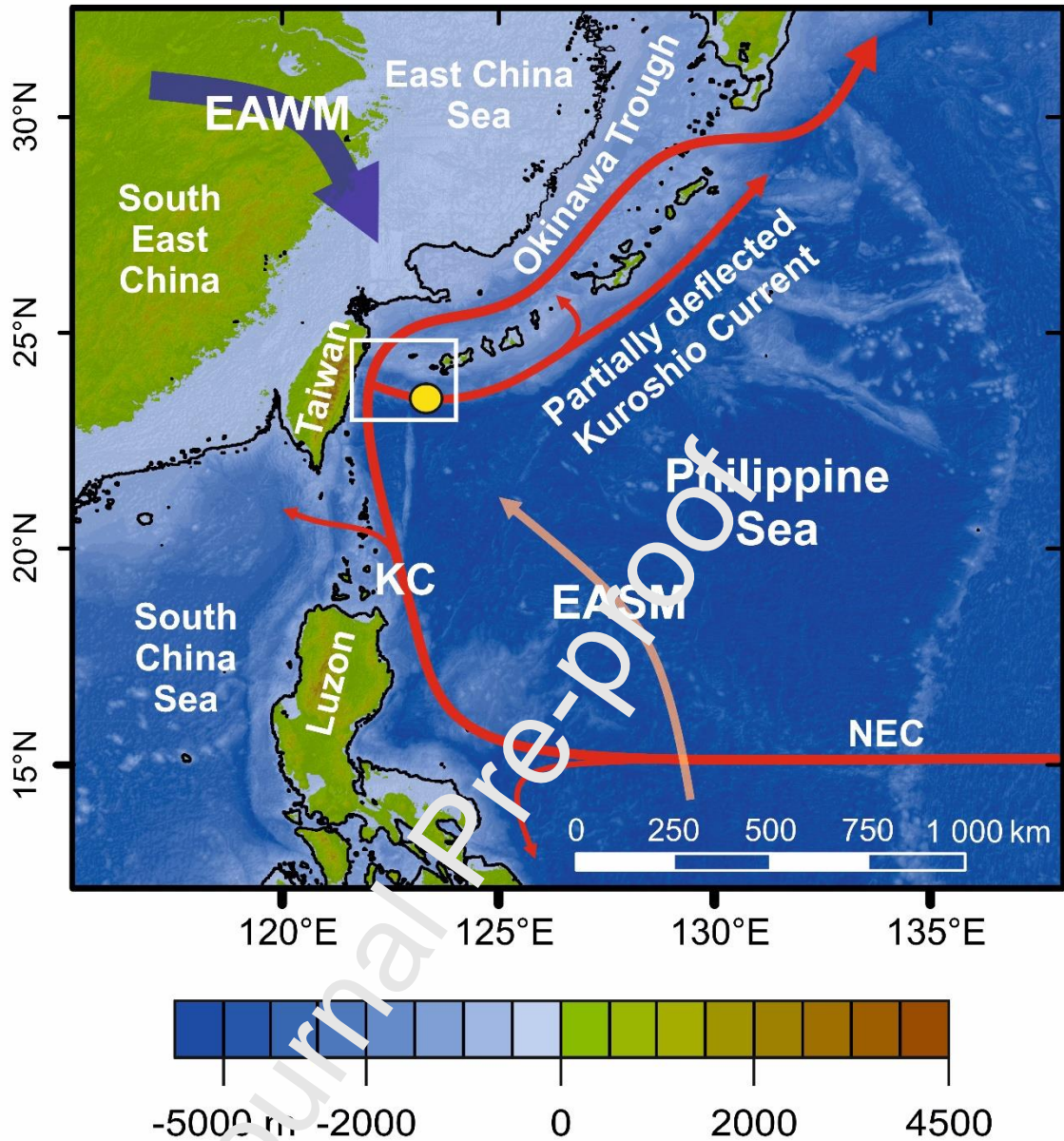


Figure 6: Proposed partial deflection of the Kuroshio Current pathway in the northwestern Philippine Sea during the Last Glacial Maximum. The 130 m isobath is marked by a thicker black line and shows the emerged area. NEC: North Equatorial Current, KC: Kuroshio Current, EASM: East Asian Summer Monsoon, EAWM: East Asian Winter Monsoon, OT: Okinawa Through.

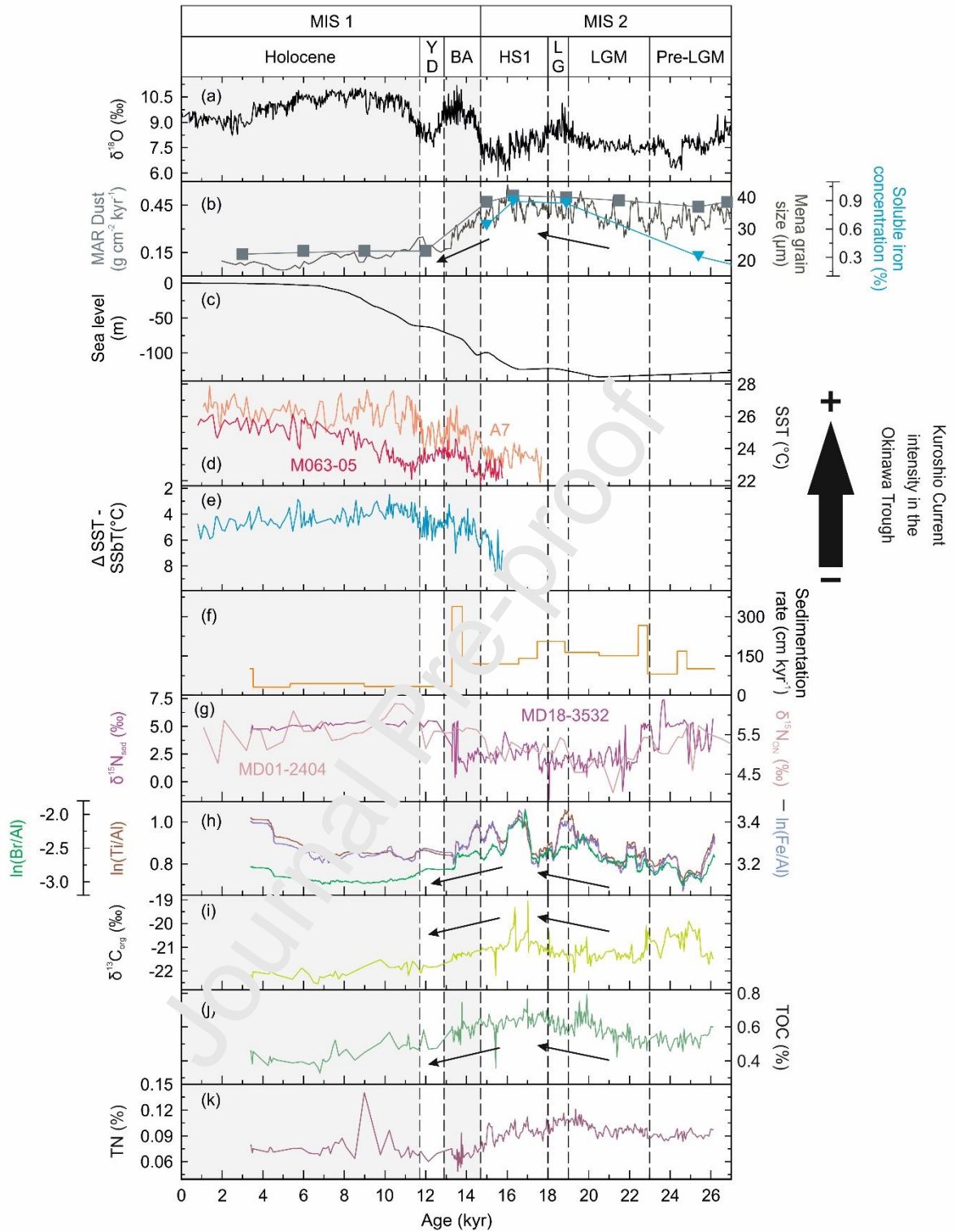


Figure 7: Variability of sedimentological and geochemical proxies with the evolution of East Asian Monsoon, relative sea level and Kuroshio Current: (a) $\delta^{18}\text{O}$ of speleothems from Hulu and Dongge caves represents the evolution of the East Asian Summer Monsoon (Cheng et

al., 2016), (b) Gulang Loess mean grain size (μm) shows changes in the intensity of the East Asian Winter Monsoon (EAWM), dust mass accumulation rate (MAR) and soluble iron concentration shows respectively the amount of dust ($\text{g cm}^{-2} \text{ kyr}^{-1}$) and soluble iron (%) brought to the ocean from the Chinese Loess Plateau by the EAWM winds in core MD06-3047, east of the Philippines (Xu et al., 2015; Fig. 1a), (c) relative sea level (m) (Lambeck et al., 2014), (d) sea surface temperature (SST) in $^{\circ}\text{C}$ respectively based on Mg/Ca and UK'₃₇ measurements in core A7 (red) (Sun et al., 2005) and M063-05 (orange) (Li et al., 2020) as an indicator of the Kuroshio Current intensity in the middle of the Okinawa Trough (Fig. 1a), (e) relative annual mean depth of the thermocline reconstructed using the temperature differences between SST and Sea Subsurface Temperature (SSbT) in $^{\circ}\text{C}$ respectively based on UK'₃₇ and TEX⁸⁶_H from core M063-05 (Fig. 1a) as an indicator of the Kuroshio Current intensity in the middle of the Okinawa Trough (Li et al., 2020). The following data are all from core MD18-3532: (f) sedimentation rate (cm kyr^{-1}), (g) $\delta^{15}\text{N}_{\text{sedimentary}}$ (‰) in core MD18-3532 (this study) and $\delta^{15}\text{N}_{\text{Organic Nitrogen}}$ (‰) in core MD01-2404 (Zheng et al., 2015; Fig. 1a), (h) elemental ratios with $\ln(\text{Br}/\text{Al})$ indicating marine organic matter; $\ln(\text{Ti}/\text{Al})$ and $\ln(\text{Fe}/\text{Al})$ showing eolian input of Fe and Ti by dust from Chinese Plateau loess, (i) $\delta^{13}\text{C}_{\text{org}}$ (‰), (j) Total Organic Carbon (TOC; %) and (k) Total Nitrogen (TN; %). The division of the time scale is first done on the scale of marine isotope stages (MIS) and then on the scale of late Quaternary millennium-scale changes with: Pre-Last Glacial Maximum (Pre-LGM), Last Glacial Maximum (LGM), Late Glacial (LG), Heinrich Stadial 1 (HS1), Bølling-Allerød (BA), Younger Dryas (YD) and Holocene. Dotted lines show the limits of each millennium-scale changes and grey areas are for warming period. Black arrows mark trends in Gulang Loess mean grain size, dust mass accumulation rate and iron soluble concentration in core MD06-3047 (b), elemental

ratios $\ln(\text{Br}/\text{Al})$, $\ln(\text{Fe}/\text{Al})$ and $\ln(\text{Ti}/\text{Al})$ (h), $\delta^{13}\text{C}_{\text{org}}$ (i) and TOC (j) from the Last Glacial Maximum to the Younger Dryas.

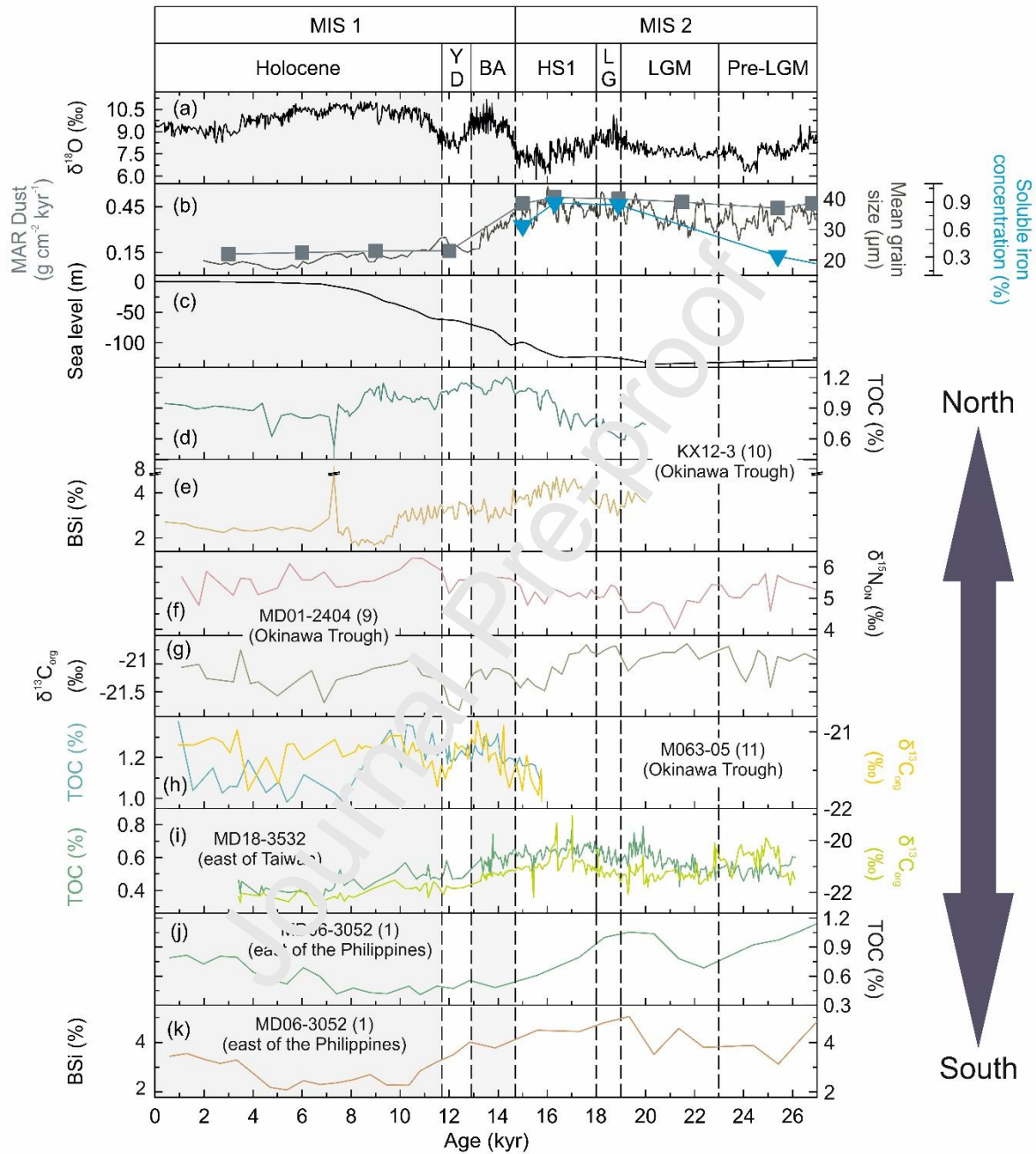


Figure 8: Spatiotemporal comparison of paleoproductivity signals along a north-south transect on the path of the Kuroshio Current (Fig. 1a): (a) $\delta^{18}\text{O}$ of speleothems from Hulu and Dongge caves represents the evolution of the East Asian Summer Monsoon (Cheng et

al., 2016), (b) Gulang Loess mean grain size (μm) shows changes in the intensity of the East Asian Winter Monsoon (EAWM), dust mass accumulation rate (MAR) and soluble iron concentration shows respectively the amount of dust ($\text{g cm}^{-2} \text{ kyr}^{-1}$) and soluble iron (%) brought to the ocean from the Chinese Loess Plateau by the EAWM winds in core MD06-3047, east of the Philippines (Xu et al., 2015; Fig. 1a), (c) relative sea level (m) (Lambeck et al., 2014), (d) Total Organic Carbon (TOC; %) in core KX12-3 (Lim et al., 2017; Fig. 1a), (e) Biogenic Silica (BSi, %) in core KX12-3 (Lim et al., 2017; Fig. 1a), (f) $\delta^{15}\text{N}_{\text{Organic Nitrogen}}$ (‰) in core MD01-2404 (Zheng et al., 2015; Fig. 1a), (g) $\delta^{13}\text{C}_{\text{Org}}$ (‰) in core MD01-2404 (Zheng et al., 2015; Fig. 1a), (h) TOC (%) and $\delta^{13}\text{C}_{\text{Org}}$ (‰) in core MD06-3052 (Chen et al., 2023; Fig. 1a), (i) TOC (%) and $\delta^{13}\text{C}_{\text{Org}}$ (‰) in core MD18-3532 (this study) (j) TOC (%) in core MD06-3052 (Xu et al., 2020; Fig. 1a) and (k) BSi (%) in core MD06-3052 (Xu et al., 2020; Fig. 1a). Numbers in brackets after the sediment core qualifier refer to the number used for core location Fig. 1a. The division of the time scale is first done on the scale of marine isotope stages (MIS) and then on the scale of late Quaternary millennium-scale changes with: Pre-Last Glacial Maximum (Pre-LGM), Last Glacial Maximum (LGM), Late Glacial (LG), Heinrich Stadial 1 (HS1), Bølling-Allerød (BA), Younger Dryas (YD) and Holocene. Dotted lines show the limits of each millennium-scale changes and grey areas are for warming period.

Supplementary material

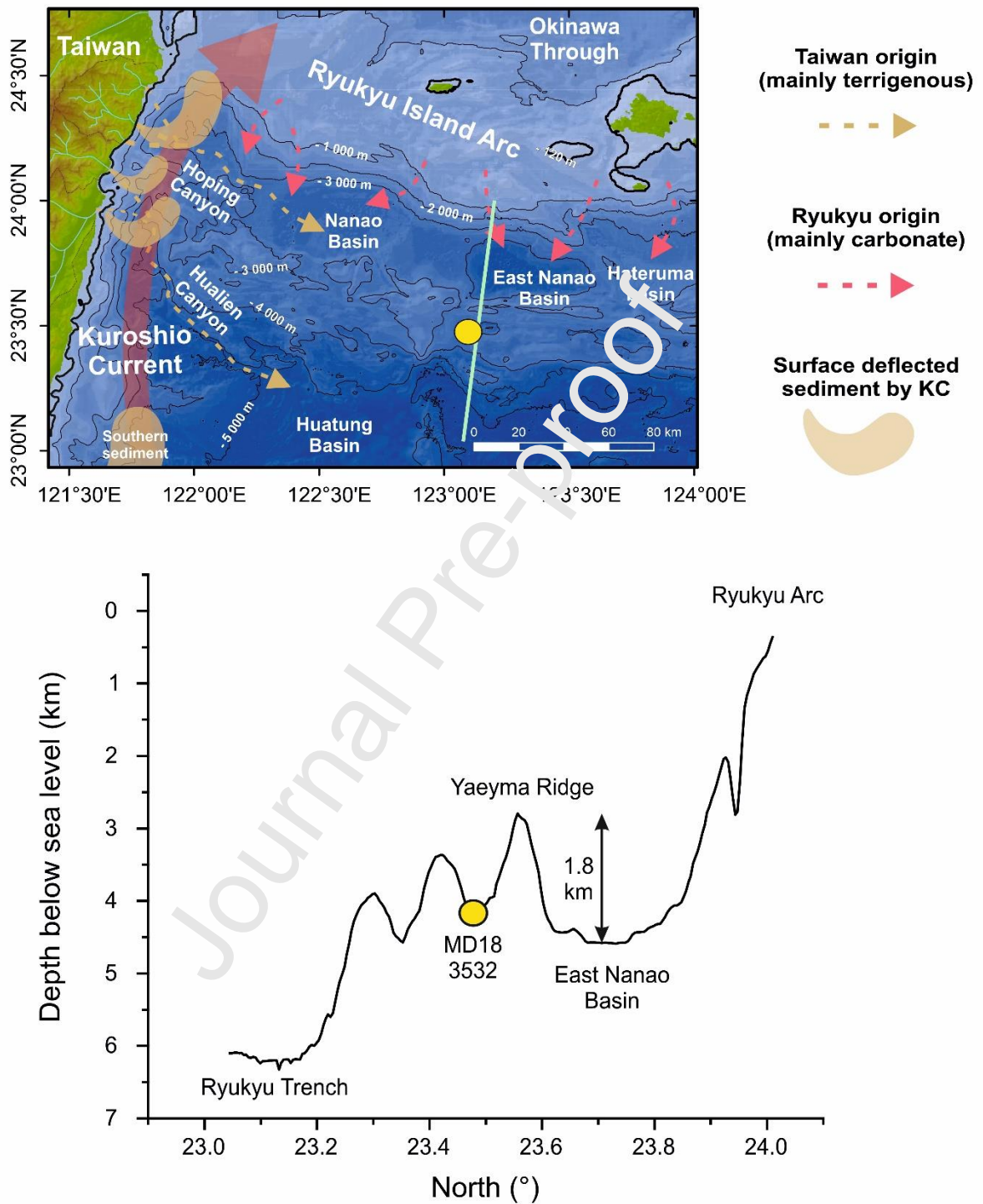


Figure S1: Bathymetric cross-section of the Ryukyu Arc up to the Ryukyu Trough represented by the light green line.

Table S1: Analytical precision and accuracy of High Organic (HO) B2151 and Low Organic (LO) B2153 standards. The theoretical expected values and errors ($\pm 2\sigma$) for $\delta^{13}\text{C}$ (‰) and $\delta^{15}\text{N}$ (‰) of the HO B2151 and LO B2153 standards are shown in the first two rows of the table. The $\delta^{13}\text{C}$ (‰) and $\delta^{15}\text{N}$ (‰) measured values of the standards and their errors are reported on the last two rows and were obtained by calculating the mean and standard deviation ($\pm 2\sigma$) of the values measured at the beginning and end of the analysis series.

	$\delta^{13}\text{C}$ (‰)	Error ($\pm 2\sigma$, ‰)	$\delta^{15}\text{N}$ (‰)	Error ($\pm 2\sigma$, ‰)
HO B2151 expected	-26.27	0.15	4.42	0.29
LO B2153 expected	-26.66	0.24	7.50	0.10
HO B2151 measured	-26.31	0.21	4.43	0.49
LO B2153 measured	-26.61	0.26	7.13	0.54

Table S2: Spearman correlation matrix of $\ln(\text{Br}/\text{Al})$, $\ln(\text{Fe}/\text{Al})$ and $\ln(\text{Ti}/\text{Al})$. Values in bold have a p-value < 0.05.

Variables	Br/Al	Fe/Al	Ti/Al
Br/Al	1	.64	.65
Fe/Al		1	.91
Ti/Al			1

Table S3: Spearman correlation matrix of $\ln(\text{Br}/\text{Al})$, $\ln(\text{Fe}/\text{Al})$ and $\ln(\text{Ti}/\text{Al})$ after smoothing by a 30-order moving average. Values in bold have a p-value < 0.05.

Variables	M30(Br /Al)	M30(Fe /Al)	M30(Ti /Al)
M30(Br /Al)	1	0.74	0.74
M30(Fe /Al)		1	0.97
M30(Ti /Al)			1

Table S4: Spearman correlation matrix of Illite, $\delta^{15}\text{N}_{\text{sed}}$ and Total N. Values in bold have a p-value < 0.05.

Variables	Illite	$\delta^{15}\text{N}_{\text{sed}}$	TN
Illite	1	0,1	-
$\delta^{15}\text{N}$		1	-
TN		0,3	1

The very large sediment export results in high sedimentation rate in the coastal regions of Taiwan. Thus, north of Taiwan, in the southern Okinawa Trough, the core MD05-2908 (5 in Fig. 1a) shows a mean sedimentation rate of 500 cm.kyr^{-1} over the last 7 kyr (Li et al., 2009). Nearby, the ODP site 1202B (6) shows sedimentation rate of 382 cm.kyr^{-1} in average during the Holocene (Wei et al., 2005). South of Taiwan, the core MD10-3291 (3) located on the west flank of the Gaoping Canyon shows a mean sedimentation of 122 cm.kyr^{-1} over the last 12 kyr (Yu et al., 2017). By contrast, during the same period, areas further away from Taiwan show lower sedimentation rates. For example, cores MD55 (7) and RN93-PC6 (8), located further north in the southern part of the Okinawa Trough than the ODP 1202B and MD05-2908 sites, have average sedimentation rates of 60 and 47 cm.kyr^{-1} (Li et al., 2009; Ujiie et al., 2003), respectively. Eastern of Taiwan, core OR1715-21 (4) located on the northern slope of the Green Island, disconnected from Taiwanese canyons inputs, shows a sedimentation rate of 25.6 cm.kyr^{-1} (Lo et al., 2013).

8 Bibliography

- Addinsoft, P., 2016. XLSTAT 2016: data analysis and statistical solution for Microsoft Excel.
- Breitbarth, E., Oschlies, A., LaRoche, J., 2007. Physiological constraints on the global distribution of *Trichodesmium* – effect of temperature on diazotrophy. *Biogeosciences* 4, 53–61. <https://doi.org/10.5194/bg-4-53-2007>
- Browning, T.J., Liu, X., Zhang, R., Wen, Z., Liu, J., Zhou, Y., Xu, F., Cai, Y., Zhou, K., Cao, Z., Zhu, Y., Shi, D., Achterberg, E.P., Dai, M., 2022. Nutrient co-limitation in the subtropical Northwest Pacific. *Limnol. Oceanogr. Lett.* 7, 52–61. <https://doi.org/10.1002/lol2.10205>
- Calvert, S.E., Pedersen, T.F., 2007. Chapter Fourteen Elemental Proxies for Palaeoclimatic and Palaeoceanographic Variability in Marine Sediments: Interpretation and Application, in: *Developments in Marine Geology*, Elsevier, pp. 567–644. [https://doi.org/10.1016/S1572-5480\(07\)01019-6](https://doi.org/10.1016/S1572-5480(07)01019-6)
- Chamley, H., 1989. *Clay Sedimentology*. Springer, Berlin, Heidelberg. <https://doi.org/10.1007/978-3-642-85916-8>
- Channell, J.E.T., Xuan, C., Hodell, D.A., Crowhurst, S.J., Larter, R.D., 2019. Relative paleointensity (RPI) and age control in Quaternary sediment drifts off the Antarctic Peninsula. *Quat. Sci. Rev.* 211, 17–33. <https://doi.org/10.1016/j.quascirev.2019.03.006>
- Chen, C.-C., Jan, S., Kuo, T.-H., Li, S.-Y., 2017. Nutrient flux and transport by the Kuroshio east of Taiwan. *J. Mar. Syst.* 167, 43–54. <https://doi.org/10.1016/j.jmarsys.2016.11.004>
- Chen, C.-C., Lu, C.-Y., Jan, S., Hsieh, C., Chung, C.-C., 2022. Effects of the Coastal Uplift on the Kuroshio Ecosystem, Eastern Taiwan, the Western Boundary Current of the North Pacific Ocean. *Front. Mar. Sci.* 9, 796187. <https://doi.org/10.3389/fmars.2022.796187>
- Chen, C.-S., Chen, Y.-L., 2003. The Rainfall Characteristics of Taiwan. *Mon. Weather Rev.* 131, 1323–1341. [https://doi.org/10.1175/1520-0493\(2003\)131<1323:TRCOT>2.0.CO;2](https://doi.org/10.1175/1520-0493(2003)131<1323:TRCOT>2.0.CO;2)
- Chen, C.-T.A., Huang, T.-H., Wu, C.-H., Yang, H., Guo, X., 2021. Variability of the nutrient stream near Kuroshio's origin. *Sci. Rep.* 11, 5080. <https://doi.org/10.1038/s41598-021-84420-5>
- Chen, C.-T.A., Liu, C.T., Pai, S.C., 1995. Variations in oxygen, nutrient and carbonate fluxes of the Kuroshio Current. *La mer* 33, 161–176.
- Chen, J.-M., Li, T., Shih, C.-F., 2010. Tropical Cyclone– and Monsoon-Induced Rainfall Variability in Taiwan. *J. Clim.* 23, 4107–4120. <https://doi.org/10.1175/2010JCLI3355.1>
- Chen, M., Li, D.-W., Li, L., Jin, G., Li, G., Xu, J., Zhao, M., 2023. Phytoplankton productivity and community structure changes in the middle Okinawa Trough since the last deglaciation. *Palaeogeogr. Palaeoclimatol. Palaeoecol.* 610, 111349. <https://doi.org/10.1016/j.palaeo.2022.111349>
- Chen, Y., Sun, X., Zhun, M., 2018. Net-phytoplankton communities in the Western Boundary Currents and their environmental correlations. *J. Oceanol. Limnol.* 36, 305–316. <https://doi.org/10.1007/s00343-017-6261-8>
- Chen, Y.L., 2000. Comparisons of primary productivity and phytoplankton size structure in the marginal regions of southern East China Sea. *Cont. Shelf Res.* 20, 437–458. [https://doi.org/10.1016/S0278-4343\(99\)00080-1](https://doi.org/10.1016/S0278-4343(99)00080-1)
- Chen, Y.L., Chen, H.-Y., Tuo, S., Ohki, K., 2008. Seasonal dynamics of new production from *Trichodesmium* N₂ fixation and nitrate uptake in the upstream Kuroshio and South

- China Sea basin. *Limnol. Oceanogr.* 53, 1705–1721.
<https://doi.org/10.4319/lo.2008.53.5.1705>
- Cheng, H., Edwards, R.L., Sinha, A., Spötl, C., Yi, L., Chen, S., Kelly, M., Kathayat, G., Wang, X., Li, X., Kong, X., Wang, Y., Ning, Y., Zhang, H., 2016. The Asian monsoon over the past 640,000 years and ice age terminations. *Nature* 534, 640–646.
<https://doi.org/10.1038/nature18591>
- Ching, K.-E., Hsieh, M.-L., Johnson, K.M., Chen, K.-H., Rau, R.-J., Yang, M., 2011. Modern vertical deformation rates and mountain building in Taiwan from precise leveling and continuous GPS observations, 2000–2008. *J. Geophys. Res. Solid Earth* 116, B08406.
<https://doi.org/10.1029/2011JB008242>
- Clark, P.U., Shakun, J.D., Baker, P.A., Bartlein, P.J., Brewer, S., Brook, E., Carlson, A.E., Cheng, H., Kaufman, D.S., Liu, Z., 2012. Global climate evolution during the last deglaciation. *Proc. Natl. Acad. Sci.* 109, E1134–E1142. <https://doi.org/10.1073/pnas.1116619109>
- Clement, A.C., Seager, R., Cane, M.A., 1999a. Orbital controls on the El Niño/Southern Oscillation and the tropical climate. *Paleoceanography* 14, 441–456.
<https://doi.org/10.1029/1999PA900013>
- Clement, A.C., Seager, R., Cane, M.A., 1999b. Orbital controls on the El Niño/Southern Oscillation and the tropical climate. *Paleoceanography* 14, 441–456.
<https://doi.org/10.1029/1999PA900013>
- Croudace, I.W., Rothwell, R.G. (Eds.), 2015. *Micro XRF Studies of Sediment Cores: Applications of a non-destructive tool for the environmental sciences*, Developments in Paleoenvironmental Research. Springer Netherlands, Dordrecht.
<https://doi.org/10.1007/978-94-017-3843-5>
- Dadson, S., Hovius, N., Pegg, S., Dade, W.B., Horng, M.J., Chen, H., 2005. Hyperpycnal river flows from an active mountain belt. *J. Geophys. Res. Earth Surf.* 110, F04016.
<https://doi.org/10.1029/2004JF000244>
- Dadson, S.J., Hovius, N., Chen, H., Dade, W.B., Hsieh, M.-L., Willett, S.D., Hu, J.-C., Horng, M.-J., Chen, M.-C., Stark, C.F., Logue, D., Lin, J.-C., 2003. Links between erosion, runoff variability and seismicity in the Taiwan orogen. *Nature* 426, 648–651.
<https://doi.org/10.1038/nature02150>
- Das, P., Lin, A.T.-S., Chen, M.-P., Miramontes, E., Liu, C.-S., Huang, N.-W., Kung, J., Hsu, S.-K., Pillutla, R.K., Nairak, K., 2021. Deep-sea submarine erosion by the Kuroshio Current in the Mariana accretionary prism, offshore Southern Taiwan. *Tectonophysics* 807, 228813. <https://doi.org/10.1016/j.tecto.2021.228813>
- Denton, G.H., Anderson, R.F., Toggweiler, J.R., Edwards, R.L., Schaefer, J.M., Putnam, A.E., 2010. The Last Glacial Termination. *Science* 328, 1652–1656.
<https://doi.org/10.1126/science.1184119>
- Dezileau, L., Lehu, R., Lallemand, S., Hsu, S.-K., Babonneau, N., Ratzov, G., Lin, A.T., Dominguez, S., 2016. Historical Reconstruction of Submarine Earthquakes Using ^{210}Pb , ^{137}Cs , and ^{241}Am Turbidite Chronology and Radiocarbon Reservoir Age Estimation off East Taiwan. *Radiocarbon* 58, 25–36.
<https://doi.org/10.1017/RDC.2015.3>
- Diekmann, B., Hofmann, J., Henrich, R., Fütterer, D.K., Röhl, U., Wei, K.-Y., 2008. Detrital sediment supply in the southern Okinawa Trough and its relation to sea-level and Kuroshio dynamics during the late Quaternary. *Mar. Geol.* 255, 83–95.
<https://doi.org/10.1016/j.margeo.2008.08.001>

- Dong, J., Li, A., Liu, X., Wan, S., Xu, F., Shi, X., 2020. Holocene Climate Modulates Mud Supply, Transport, and Sedimentation on the East China Sea Shelf. *J. Geophys. Res. Earth Surf.* 125, e2020JF005731. <https://doi.org/10.1029/2020JF005731>
- Dou, Y., Yang, S., Liu, Z., Clift, P.D., Yu, H., Berne, S., Shi, X., 2010. Clay mineral evolution in the central Okinawa Trough since 28ka: Implications for sediment provenance and paleoenvironmental change. *Palaeogeogr. Palaeoclimatol. Palaeoecol.* 288, 108–117. <https://doi.org/10.1016/j.palaeo.2010.01.040>
- Dou, Y., Yang, S., Liu, Z., Shi, X., Li, J., Yu, H., Berne, S., 2012. Sr–Nd isotopic constraints on terrigenous sediment provenances and Kuroshio Current variability in the Okinawa Trough during the late Quaternary. *Palaeogeogr. Palaeoclimatol. Palaeoecol.* 365–366, 38–47. <https://doi.org/10.1016/j.palaeo.2012.09.003>
- Eberl, R., Carpenter, E., 2007. Association of the copepod *Macrosetella gracilis* with the cyanobacterium *Trichodesmium* spp. in the North Pacific Gyre. *Mar. Ecol. Prog. Ser.* 333, 205–212. <https://doi.org/10.3354/meps333205>
- Ford, H.L., Ravelo, A.C., Polissar, P.J., 2015. Reduced El Niño–Southern Oscillation during the Last Glacial Maximum. *Science* 347, 255–258. <https://doi.org/10.1126/science.1258437>
- Fujiwara, K., Kawamura, R., Kawano, T., 2020. Remote Thermodynamic Impact of the Kuroshio Current on a Developing Tropical Cyclone Over the Western North Pacific in Boreal Fall. *J. Geophys. Res. Atmospheres* 125, e2019JD031356. <https://doi.org/10.1029/2019JD031356>
- Galbraith, E.D., Kienast, M., Jaccard, S.L., Pedersen, T.F., Brunelle, B.G., Sigman, D.M., Kiefer, T., 2008. Consistent relationship between global climate and surface nitrate utilization in the western subarctic Pacific throughout the last 500 ka. *Paleoceanography* 23, PA2212. <https://doi.org/10.1029/2007PA001518>
- Goericke, R., Fry, B., 1994. Variations of marine plankton $\delta^{13}\text{C}$ with latitude, temperature, and dissolved CO_2 in the world ocean. *Glob. Biogeochem. Cycles* 8, 85–90. <https://doi.org/10.1029/93GB03272>
- Govin, A., Holzwarth, U., Heslop, D., Ford Keeling, L., Zabel, M., Mulitza, S., Collins, J.A., Chiessi, C.M., 2012. Distribution of major elements in Atlantic surface sediments (36°N–49°S): Imprint of terrigenous input and continental weathering. *Geochem. Geophys. Geosystems* 13. <https://doi.org/10.1029/2011GC003785>
- Gray, W.M., 1977. Tropical cyclone genesis in the western North Pacific. *J. Meteorol. Soc. Jpn. Ser II* 55, 465–482.
- Guo, X., Zhu, X.-H., Wu, Q.-S., Huang, D., 2012. The Kuroshio nutrient stream and its temporal variation in the East China Sea. *J. Geophys. Res. Oceans* 117. <https://doi.org/10.1029/2011JC007292>
- Harvey, G.R., 1980. A study of the chemistry of iodine and bromine in marine sediments. *Mar. Chem.* 8, 327–332. [https://doi.org/10.1016/0304-4203\(80\)90021-3](https://doi.org/10.1016/0304-4203(80)90021-3)
- He, J., Zhao, M., Wang, P., Li, L., Li, Q., 2013. Changes in phytoplankton productivity and community structure in the northern South China Sea during the past 260ka. *Palaeogeogr. Palaeoclimatol. Palaeoecol.* 392, 312–323. <https://doi.org/10.1016/j.palaeo.2013.09.010>
- He, M., Zheng, H., Huang, X., Jia, J., Li, L., 2013. Yangtze River sediments from source to sink traced with clay mineralogy. *J. Asian Earth Sci., New Global Perspectives on Paleontology, Stratigraphy, Paleoceanography, Paleoclimatology, and Tectonics in*

- the East Asia and Western Pacific 69, 60–69.
<https://doi.org/10.1016/j.jseaes.2012.10.001>
- He, S., Cheng, X., Fei, J., Wei, Z., Huang, X., Liu, L., 2022. Thermal Response to Tropical Cyclones Over the Kuroshio. *Earth Space Sci.* 9, e2021EA002001.
<https://doi.org/10.1029/2021EA002001>
- Heaton, T.J., Köhler, P., Butzin, M., Bard, E., Reimer, R.W., Austin, W.E.N., Bronk Ramsey, C., Grootes, P.M., Hughen, K.A., Kromer, B., Reimer, P.J., Adkins, J., Burke, A., Cook, M.S., Olsen, J., Skinner, L.C., 2020. Marine20—The Marine Radiocarbon Age Calibration Curve (0–55,000 cal BP). *Radiocarbon* 62, 779–820.
<https://doi.org/10.1017/RDC.2020.68>
- Held, N.A., Webb, E.A., McIlvin, M.M., Hutchins, D.A., Cohen, N.R., Moran, D.M., Kunde, K., Lohan, M.C., Mahaffey, C., Woodward, E.M.S., Saito, M.A., 2020. Co-occurrence of Fe and P stress in natural populations of the marine diazotroph *Trichodesmium*. *Biogeosciences* 17, 2537–2551. <https://doi.org/10.5194/bg-17-2537-2020>
- Hillenbrand, C.-D., Crowhurst, S.J., Williams, M., Hodell, D.A., McCave, I.N., Ehrmann, W., Xuan, C., Piotrowski, A.M., Hernández-Molina, F.J., Graham, A.G.C., Grobe, H., Williams, T.J., Horrocks, J.R., Allen, C.S., Larter, R.D., 2021. New insights from multi-proxy data from the West Antarctic continental rise: Implications for dating and interpreting Late Quaternary palaeoenvironmental records. *Quat. Sci. Rev.* 257, 106842. <https://doi.org/10.1016/j.quascirev.2021.106842>
- Hilton, R.G., Galy, A., Hovius, N., Horng, M.-J., Chen, H., 2010. The isotopic composition of particulate organic carbon in mountain rivers of Taiwan. *Geochim. Cosmochim. Acta* 74, 3164–3181. <https://doi.org/10.1016/j.gca.2010.03.004>
- Ho, C.S., 1986. A synthesis of the geologic evolution of Taiwan. *Tectonophysics, Geodynamics of the Eurasia-Philippine Sea Plate Boundary* 125, 1–16.
[https://doi.org/10.1016/0040-1951\(86\)90004-1](https://doi.org/10.1016/0040-1951(86)90004-1)
- Hollstein, M., Mohtadi, M., Rosenthal, Y., Prange, M., Oppo, D.W., Martínez Méndez, G., Tachikawa, K., Moffa Sánchez, P., Steinke, S., Hebbeln, D., 2018. Variations in Western Pacific Warm Pool surface and thermocline conditions over the past 110,000 years: Forcing mechanisms and implications for the glacial Walker circulation. *Quat. Sci. Rev.* 201, 429–445. <https://doi.org/10.1016/j.quascirev.2018.10.030>
- Horng, C.S., Huh, C.A., Chen, K.H., Lin, C.H., Shea, K.S., Hsiung, K.H., 2012. Pyrrhotite as a tracer for denudation of the Taiwan orogen. *Geochem. Geophys. Geosystems* 13, undefined-undefined. <https://doi.org/10.1029/2012GC004195>
- Hsiung, K.-H., Kanamatsu, T., Ikehara, K., Shiraishi, K., Horng, C.-S., Usami, K., 2017. Morpho-sedimentary features and sediment dispersal systems of the southwest end of the Ryukyu Trench: a source-to-sink approach. *Geo-Mar. Lett.* 37, 561–577.
<https://doi.org/10.1007/s00367-017-0509-3>
- Hsu, Y.-J., Lai, Y.-R., You, R.-J., Chen, H.-Y., Teng, L.S., Tsai, Y.-C., Tang, C.-H., Su, H.-H., 2018. Detecting rock uplift across southern Taiwan mountain belt by integrated GPS and leveling data. *Tectonophysics* 744, 275–284.
<https://doi.org/10.1016/j.tecto.2018.07.012>
- Hu, D., Wu, L., Cai, W., Gupta, A.S., Ganachaud, A., Qiu, B., Gordon, A.L., Lin, X., Chen, Z., Hu, S., Wang, G., Wang, Q., Sprintall, J., Qu, T., Kashino, Y., Wang, F., Kessler, W.S., 2015. Pacific western boundary currents and their roles in climate. *Nature* 522, 299–308.
<https://doi.org/10.1038/nature14504>

- Huang, C., Zhao, W., Liu, F., Tan, W., Koopal, L.K., 2011. Environmental significance of mineral weathering and pedogenesis of loess on the southernmost Loess Plateau, China. *Geoderma* 163, 219–226. <https://doi.org/10.1016/j.geoderma.2011.04.018>
- Huang, E., Tian, J., Steinke, S., 2011. Millennial-scale dynamics of the winter cold tongue in the southern South China Sea over the past 26ka and the East Asian winter monsoon. *Quat. Res.* 75, 196–204. <https://doi.org/10.1016/j.yqres.2010.08.014>
- Jaboyedoff, M., Bussy, F., Kübler, B., Thelin, Ph., 2001. Illite “Crystallinity” Revisited. *Clays Clay Miner.* 49, 156–167. <https://doi.org/10.1346/CCMN.2001.0490205>
- Jan, S., Yang, Y.J., Wang, J., Mensah, V., Kuo, T.-H., Chiou, M.-D., Chern, C.-S., Chang, M.-H., Chien, H., 2015. Large variability of the Kuroshio at 23.75°N east of Taiwan. *J. Geophys. Res. Oceans* 120, 1825–1840. <https://doi.org/10.1002/2014JC010614>
- Ji, J., Chen, J., Lu, H., 1999. Origin of illite in the loess from the Luochuan area, Loess Plateau, Central China. *Clay Miner.* 34, 525–532. <https://doi.org/10.1180/000985599546398>
- Jiang, F., Zhou, Ye, Nan, Q., Zhou, Yu, Zheng, X., Li, T., Li, A., Wang, H., 2016. Contribution of Asian dust and volcanic material to the western Philippine Sea over the last 220 kyr as inferred from grain size and Sr-Nd isotopes: DUST AND VOLCANIC MATERIAL CONTRIBUTION. *J. Geophys. Res. Oceans* 121, 6911–6928. <https://doi.org/10.1002/2016JC012000>
- Jiang, Z., Chen, J., Zhai, H., Zhou, F., Yan, X., Zhu, Y., Xuan, J., Shou, L., Chen, Q., 2019. Kuroshio Shape Composition and Distribution of Filamentous Diazotrophs in the East China Sea and Southern Yellow Sea. *J. Geophys. Res. Oceans* 124, 7421–7436. <https://doi.org/10.1029/2019JC015413>
- Kandasamy, S., Lin, B., Lou, J.-Y., Kao, S.-J., Chen, C.-T.A., Mayer, L.M., 2018. Estimation of Marine Versus Terrigenous Organic Carbon in Sediments Off Southwestern Taiwan Using the Bromine to Total Organic Carbon Ratio as a Proxy. *J. Geophys. Res. Biogeosciences* 123, 3387–3402. <https://doi.org/10.1029/2018JG004674>
- Kao, S.-J., Hilton, R.G., Selvaraj, K., Dai, M., Zehetner, F., Huang, J.-C., Hsu, S.-C., Sparkes, R., Liu, J.T., Lee, T.-Y., Yang, J.-T., Galy, A., Xu, X., Hovius, N., 2014. Preservation of terrestrial organic carbon in marine sediments offshore Taiwan: mountain building and atmospheric carbon dioxide sequestration. *Earth Surf. Dyn.* 2, 127–139. <https://doi.org/10.5194/esurf-2-127-2014>
- Kao, S.J., Lin, F.J., Liu, K.K., 2003. Organic carbon and nitrogen contents and their isotopic compositions in surficial sediments from the East China Sea shelf and the southern Okinawa Trough. *Deep Sea Res. Part II Top. Stud. Oceanogr., Circulation and biogeochemical processes in the East China Sea and the vicinity of Taiwan* 50, 1203–1217. [https://doi.org/10.1016/S0967-0645\(03\)00018-3](https://doi.org/10.1016/S0967-0645(03)00018-3)
- Kim, R.A., Lee, K.E., Bae, S.W., 2015. Sea surface temperature proxies (alkenones, foraminiferal Mg/Ca, and planktonic foraminiferal assemblage) and their implications in the Okinawa Trough. *Prog. Earth Planet. Sci.* 2, 43. <https://doi.org/10.1186/s40645-015-0074-1>
- Kim, S., Khim, B.-K., Ikehara, M., Takahashi, K., 2017. Relationship between $\delta^{15}\text{N}$ values of bulk sediments and total organic carbon concentration in response to orbital-scale biogenic opal production in the Bering slope area over the last 600 kyrs. *Quat. Int., Marine Geology in Asian Marginal Seas: ICAMG-8* 459, 144–152. <https://doi.org/10.1016/j.quaint.2017.05.041>

- Kneller, B., Buckee, C., 2000. The structure and fluid mechanics of turbidity currents: a review of some recent studies and their geological implications. *Sedimentology* 47, 62–94. <https://doi.org/10.1046/j.1365-3091.2000.047s1062.x>
- Kodama, T., Shimizu, Y., Ichikawa, T., Hiroe, Y., Kusaka, A., Morita, H., Shimizu, M., Hidaka, K., 2014. Seasonal and spatial contrast in the surface layer nutrient content around the Kuroshio along 138°E, observed between 2002 and 2013. *J. Oceanogr.* 70, 489–503. <https://doi.org/10.1007/s10872-014-0245-5>
- Koutavas, A., Lynch-Stieglitz, J., Marchitto, T.M., Sachs, J.P., 2002. El Niño-Like Pattern in Ice Age Tropical Pacific Sea Surface Temperature. *Science* 297, 226–230. <https://doi.org/10.1126/science.1072376>
- Kutzbach, J.E., 1993. Simulated climatic changes: results of the COHMAP climate-model experiments. *Glob. Clim. Last Glacial Maximum* 24–93.
- Lambeck, K., Rouby, H., Purcell, A., Sun, Y., Sambridge, M., 2014. Sea level and global ice volumes from the Last Glacial Maximum to the Holocene. *Proc. Natl. Acad. Sci.* 111, 15296–15303. <https://doi.org/10.1073/pnas.1411762111>
- Li, C., Jiang, B., Li, A., Li, T., Jiang, F., 2009. Sedimentation rates and provenance analysis in the Southwestern Okinawa Trough since the mid-Holocene. *Sci. Bull.* 54, 1234–1242. <https://doi.org/10.1007/s11434-009-0010-0>
- Li, C., Shi, X., Kao, S., Chen, M., Liu, Y., Fang, X., Lü, H., Zou, J., Liu, S., Qiao, S., 2012. Clay mineral composition and their sources for the fluvial sediments of Taiwanese rivers. *Chin. Sci. Bull.* 57, 673–681. <https://doi.org/10.1007/s11434-011-4824-1>
- Li, C.-F., Chytry, M., Zelený, D., Chen, J.-J., Chen, T.-Y., Chiou, C.-R., Hsia, Y., Liu, H.-Y., Sheng-Zehn, Y., Yeh, C., Wang, J.-C., Yu, C.-F., Lai, Y.-J., Chao, W.-C., Hsieh, C.-F., 2013. Classification of Taiwan forest vegetation. *Appl. Veg. Sci.* 16, 698–719. <https://doi.org/10.1111/avsc.12025>
- Li, Q., Li, G., Chen, M.-T., Xu, J., Liu, C., Chen, M., 2020. New Insights Into Kuroshio Current Evolution Since the Last Deglaciation Based on Paired Organic Paleothermometers From the Middle Okinawa Trough. *Paleoceanogr. Paleoclimatology* 35, e2020PA004140. <https://doi.org/10.1029/2020PA004140>
- Li, Q., Zhang, Q., Li, G., Liu, C., Chen, M.-T., Xu, J., Li, J., 2019. A new perspective for the sediment provenance evolution of the middle Okinawa Trough since the last deglaciation based on integrated methods. *Earth Planet. Sci. Lett.* 528, 115839. <https://doi.org/10.1016/j.epsl.2019.115839>
- Lim, D., Kim, J., Xu, Z., Jeong, K., Jung, H., 2017. New evidence for Kuroshio inflow and deepwater circulation in the Okinawa Trough, East China Sea: Sedimentary mercury variations over the last 20 kyr. *Paleoceanography* 32, 571–579. <https://doi.org/10.1002/2017PA003116>
- Lis, H., Kranzler, C., Keren, N., Shaked, Y., 2015. A Comparative Study of Iron Uptake Rates and Mechanisms amongst Marine and Fresh Water Cyanobacteria: Prevalence of Reductive Iron Uptake. *Life* 5, 841–860. <https://doi.org/10.3390/life5010841>
- Liu, J., Xiang, R., Kao, S.-J., Fu, S., Zhou, L., 2016. Sedimentary responses to sea-level rise and Kuroshio Current intrusion since the Last Glacial Maximum: Grain size and clay mineral evidence from the northern South China Sea slope. *Palaeogeogr. Palaeoclimatol. Palaeoecol.* 450, 111–121. <https://doi.org/10.1016/j.palaeo.2016.03.002>
- Liu, J.P., Li, A.C., Xu, K.H., Velozzi, D.M., Yang, Z.S., Milliman, J.D., DeMaster, D.J., 2006. Sedimentary features of the Yangtze River-derived along-shelf clinof orm deposit in

- the East China Sea. *Cont. Shelf Res., Special Issue in Honor of Richard W. Sternberg's Contributions to Marine Sedimentology* 26, 2141–2156. <https://doi.org/10.1016/j.csr.2006.07.013>
- Liu, K.-K., Su, M.-J., Hsueh, C.-R., Gong, G.-C., 1996. The nitrogen isotopic composition of nitrate in the Kuroshio Water northeast of Taiwan: evidence for nitrogen fixation as a source of isotopically light nitrate. *Mar. Chem.* 54, 273–292. [https://doi.org/10.1016/0304-4203\(96\)00034-5](https://doi.org/10.1016/0304-4203(96)00034-5)
- Liu, X., Wei, J., 2015. Understanding surface and subsurface temperature changes induced by tropical cyclones in the Kuroshio. *Ocean Dyn.* 65, 1017–1027. <https://doi.org/10.1007/s10236-015-0851-9>
- Liu, Z., Colin, C., Li, X., Zhao, Y., Tuo, S., Chen, Z., Siringan, F.P., Liu, J.T., Huang, C.-Y., You, C.-F., Huang, K.-F., 2010. Clay mineral distribution in surface sediments of the northeastern South China Sea and surrounding fluvial drainage basins: Source and transport. *Mar. Geol.* 277, 48–60. <https://doi.org/10.1016/j.margeo.2010.08.010>
- Lo, L., Lai, Y.-H., Wei, K.-Y., Lin, Y.-S., Mii, H.-S., Shen, C.-C., 2013. Persistent sea surface temperature and declined sea surface salinity in the northwestern tropical Pacific over the past 7500 years. *J. Asian Earth Sci.* 66, 234–239. <https://doi.org/10.1016/j.jseaes.2013.01.014>
- Maher, B.A., 2016. Palaeoclimatic records of the loess/palaeosol sequences of the Chinese Loess Plateau. *Quat. Sci. Rev.* 154, 23–84. <https://doi.org/10.1016/j.quascirev.2016.08.004>
- Mann, H.B., Whitney, D.R., 1947. On a test of whether one of two random variables is stochastically larger than the other. *Ann. Math. Stat.* 50–60.
- Martinez-Ruiz, F., Kastner, M., Gallego-Forres, D., Rodrigo-Gámiz, M., Nieto-Moreno, V., Ortega-Huertas, M., 2015. Paleoclimate and paleoceanography over the past 20,000 yr in the Mediterranean Sea Basins as indicated by sediment elemental proxies. *Quat. Sci. Rev.* 107, 25–46. <https://doi.org/10.1016/j.quascirev.2014.09.018>
- Matsu'ura, T., Ikehara, M., Ueno, T., 2021. Late Quaternary tephrostratigraphy and cryptotephrostratigraphy of core MD012422: Improving marine tephrostratigraphy of the NW Pacific. *Quat. Sci. Rev.* 257, 106808. <https://doi.org/10.1016/j.quascirev.2021.106808>
- Mayer, L.M., Schick, L.L., Alison, M.A., Ruttenberg, K.C., Bentley, S.J., 2007. Marine vs. terrigenous organic matter in Louisiana coastal sediments: The uses of bromine:organic carbon ratios. *Mar. Chem.* 107, 244–254. <https://doi.org/10.1016/j.marchem.2007.07.007>
- McGee, D., Moreno-Chamarro, E., Marshall, J., Galbraith, E.D., 2018. Western U.S. lake expansions during Heinrich stadials linked to Pacific Hadley circulation. *Sci. Adv.* 4, eaav0118. <https://doi.org/10.1126/sciadv.aav0118>
- McManus, J.F., Francois, R., Gherardi, J.-M., Keigwin, L.D., Brown-Leger, S., 2004. Collapse and rapid resumption of Atlantic meridional circulation linked to deglacial climate changes. *Nature* 428, 834–837. <https://doi.org/10.1038/nature02494>
- Merkel, U., Prange, M., Schulz, M., 2010. ENSO variability and teleconnections during glacial climates. *Quat. Sci. Rev., Climate of the Last Million Years: New Insights from EPICA and Other Records* 29, 86–100. <https://doi.org/10.1016/j.quascirev.2009.11.006>
- Meyers, P.A., 1997. Organic geochemical proxies of paleoceanographic, paleolimnologic, and paleoclimatic processes. *Org. Geochem.* 27, 213–250. [https://doi.org/10.1016/S0146-6380\(97\)00049-1](https://doi.org/10.1016/S0146-6380(97)00049-1)

- Mix, A.C., Bard, E., Schneider, R., 2001. Environmental processes of the ice age: land, oceans, glaciers (EPILOG). *Quat. Sci. Rev.* 20, 627–657. [https://doi.org/10.1016/S0277-3791\(00\)00145-1](https://doi.org/10.1016/S0277-3791(00)00145-1)
- Mulder, T., Syvitski, J.P.M., Migeon, S., Faugères, J.-C., Savoye, B., 2003. Marine hyperpycnal flows: initiation, behavior and related deposits. A review. *Mar. Pet. Geol.* 20, 861–882. <https://doi.org/10.1016/j.marpetgeo.2003.01.003>
- Na, H., Wimbush, M., Park, J.-H., Nakamura, H., Nishina, A., 2014. Observations of flow variability through the Kerama Gap between the East China Sea and the Northwestern Pacific. *J. Geophys. Res. Oceans* 119, 689–703. <https://doi.org/10.1002/2013JC008899>
- Nayak, K., Garzanti, E., Lin, A.T.-S., Castelltort, S., 2022. Taiwan river muds from source to sink: Provenance control, inherited weathering, and offshore dispersal pathways. *Sediment. Geol.* 438, 106199. <https://doi.org/10.1016/j.sedgeo.2022.106199>
- Nayak, K., Lin, A.T.-S., Huang, K.-F., Liu, Z., Babonneau, N., Ratzov, G., Pillutla, R.K., Das, P., Hsu, S.-K., 2021. Clay-mineral distribution in recent deep-sea sediments around Taiwan: Implications for sediment dispersal processes. *Tectonophysics* 814, 228974. <https://doi.org/10.1016/j.tecto.2021.228974>
- Nieto-Moreno, V., Martínez-Ruiz, F., Giralt, S., Jiménez-Espejo, F., Gallego-Torres, D., Rodrigo-Gámiz, M., García-Orellana, J., Ortega-Iuertas, M., de Lange, G.J., 2011. Tracking climate variability in the western Mediterranean during the Late Holocene: a multiproxy approach. *Clim. Past* 7, 1395–1414. <https://doi.org/10.5194/cp-7-1395-2011>
- Owen, J.S., 2013. Stable Nitrogen Isotopes in a Forested Watershed in Taiwan. *J. For. Environ. Sci.* 29, 116–124. <https://doi.org/10.7747/JFS.2013.29.2.116>
- Pan, J., Feng, X., Lai, W., Devlin, A.T., Lin, H., 2018. Barrier Effects of the Kuroshio Current on the East Asian Northerly Monsoon: A Sensitivity Analysis. *Sci. Rep.* 8, 18044. <https://doi.org/10.1038/s41598-018-36577-9>
- Qiu, B., 2001. Kuroshio And Oyashio Currents, in: *Encyclopedia of Ocean Sciences*. Elsevier, pp. 1413–1425. <https://doi.org/10.1006/rwos.2001.0350>
- Qiu, B., Lukas, R., 1996. Seasonal and interannual variability of the North Equatorial Current, the Mindanao Current and the Kuroshio along the Pacific western boundary. *J. Geophys. Res. Ocean.* 101, 12315–12330. <https://doi.org/10.1029/95JC03204>
- Qiu, B., Rudnick, D.L., Cerovecki, I., Cornuelle, B.D., Chen, S., Schönau, M.C., McClean, J.L., Gopalakrishnan, C., 2015. The Pacific North Equatorial Current: New Insights from the Origins of the Kuroshio and Mindanao Currents (OKMC) Project. *Oceanography* 28, 24–33. <http://dx.doi.org/10.5670/oceanog.2015.78>
- Qiu, G.-W., Koedooder, C., Qiu, B.-S., Shaked, Y., Keren, N., 2022. Iron transport in cyanobacteria – from molecules to communities. *Trends Microbiol.* 30, 229–240. <https://doi.org/10.1016/j.tim.2021.06.001>
- Qu, T., Lukas, R., 2003. The Bifurcation of the North Equatorial Current in the Pacific. *J. Phys. Oceanogr.* 33, 5–18. [https://doi.org/10.1175/1520-0485\(2003\)033<0005:TBOTNE>2.0.CO;2](https://doi.org/10.1175/1520-0485(2003)033<0005:TBOTNE>2.0.CO;2)
- Ramsey, C.B., 2008. Deposition models for chronological records. *Quat. Sci. Rev., INTegration of Ice-core, Marine and Terrestrial records (INTIMATE): Refining the record of the Last Glacial-Interglacial Transition* 27, 42–60. <https://doi.org/10.1016/j.quascirev.2007.01.019>

- Resentini, A., Goren, L., Castelltort, S., Garzanti, E., 2017. Partitioning sediment flux by provenance and tracing erosion patterns in Taiwan. *J. Geophys. Res. Earth Surf.* 122, 1430–1454. <https://doi.org/10.1002/2016JF004026>
- Richter, T.O., van der Gaast, S., Koster, B., Vaars, A., Gieles, R., de Stigter, H.C., De Haas, H., van Weering, T.C.E., 2006. The Avaatech XRF Core Scanner: technical description and applications to NE Atlantic sediments. *Geol. Soc. Lond. Spec. Publ.* 267, 39–50. <https://doi.org/10.1144/GSL.SP.2006.267.01.03>
- Robinson, R., Kienast, M., Albuquerque, A., Altabet, M., Contreras, S., De Pol-Holz, R., Dubois, N., Francois, R., Galbraith, E., Hsu, T.-C., Ivanochko, T., Jaccard, S., Kao, S.-J., Kiefer, T., Kienast, S., Lehmann, M., Martinez, P., McCarthy, M., Moebius, J., Yang, J.-Y., 2012. A review of nitrogen isotopic alteration in marine sediments. *Paleoceanography* 27. <https://doi.org/10.1029/2012PA002321>
- Ruan, J., Xu, Y., Ding, S., Wang, Y., Zhang, X., 2017. A biomarker record of temperature and phytoplankton community structure in the Okinawa Trough since the last glacial maximum. *Quat. Res.* 88, 89–97. <https://doi.org/10.1017/qua.2017.28>
- Sanchez Goñi, M.F., Harrison, S.P., 2010. Millennial-scale climate variability and vegetation changes during the Last Glacial: Concepts and terminology. *Quat. Sci. Rev.* 29, 2823–2827. <https://doi.org/10.1016/j.quascirev.2009.11.014>
- Sasaki, Y.N., Minobe, S., Asai, T., Inatsu, M., 2012. Influence of the Kuroshio in the East China Sea on the Early Summer (Baiu) Rain. *J. Clim.* 25, 6627–6645. <https://doi.org/10.1175/JCLI-D-11-00727.1>
- Schubert, C.J., Calvert, S.E., 2001. Nitrogen and carbon isotopic composition of marine and terrestrial organic matter in Arctic Ocean sediments: implications for nutrient utilization and organic matter composition. *Deep Sea Res. Part Oceanogr. Res. Pap.* 48, 789–810. [https://doi.org/10.1016/S0967-0637\(00\)00069-8](https://doi.org/10.1016/S0967-0637(00)00069-8)
- Shiozaki, T., Takeda, S., Itoh, S., Kodama, T., Liu, X., Hashihama, F., Furuya, K., 2015. Why is *Trichodesmium* abundant in the Kuroshio? *Biogeosciences* 12, 6931–6943. <https://doi.org/10.5194/bg-12-6931-2015>
- Stein, R., 1991. Accumulation of Organic Carbon in Marine Sediments, Lecture Notes in Earth Sciences. Springer-Verlag, Berlin/Heidelberg. <https://doi.org/10.1007/BFb0010382>
- Steinke, S., Hanebuth, T.J.J., Vogt, C., Statterger, K., 2008. Sea level induced variations in clay mineral composition in the southwestern South China Sea over the past 17,000 yr. *Mar. Geol.* 250, 199–210. <https://doi.org/10.1016/j.margeo.2008.01.005>
- Steinke, S., Mohtadi, M., Groeneveld, J., Lin, L.-C., Löwemark, L., Chen, M.-T., Rendle-Bühning, R., 2010. Reconstructing the southern South China Sea upper water column structure since the Last Glacial Maximum: Implications for the East Asian winter monsoon development. *Paleoceanography* 25, PA2219. <https://doi.org/10.1029/2009PA001850>
- Sun, Y., Clemens, S.C., Morrill, C., Lin, X., Wang, X., An, Z., 2012. Influence of Atlantic meridional overturning circulation on the East Asian winter monsoon. *Nat. Geosci.* 5, 46–49. <https://doi.org/10.1038/ngeo1326>
- Sun, Y., Oppo, D.W., Xiang, R., Liu, W., Gao, S., 2005. Last deglaciation in the Okinawa Trough: Subtropical northwest Pacific link to Northern Hemisphere and tropical climate. *Paleoceanography* 20. <https://doi.org/10.1029/2004PA001061>
- Tian, Z., Jiang, D., 2020. Weakening and eastward shift of the tropical Pacific Walker circulation during the Last Glacial Maximum. *Boreas* 49, 200–210. <https://doi.org/10.1111/bor.12417>

- Timmermann, A., Lorenz, S.J., An, S.I., Clement, A., Xie, S.P., 2007. The effect of orbital forcing on the mean climate and variability of the tropical Pacific. *J. Clim.* 20, 4147–4159.
- Ujiie, H., Ujiie, Y., 1999. Late Quaternary course changes of the Kuroshio Current in the Ryukyu Arc region, northwestern Pacific Ocean. *Mar. Micropaleontol.* 37, 23–40. [https://doi.org/10.1016/S0377-8398\(99\)00010-9](https://doi.org/10.1016/S0377-8398(99)00010-9)
- Ujiie, Y., Ujiie, H., Taira, A., Nakamura, T., Oguri, K., 2003. Spatial and temporal variability of surface water in the Kuroshio source region, Pacific Ocean, over the past 21,000 years: evidence from planktonic foraminifera. *Mar. Micropaleontol.* 49, 335–364. [https://doi.org/10.1016/S0377-8398\(03\)00062-8](https://doi.org/10.1016/S0377-8398(03)00062-8)
- Verdel, C., van der Pluijm, B.A., Niemi, N., 2012. Variation of illite/muscovite $^{40}\text{Ar}/^{39}\text{Ar}$ age spectra during progressive low-grade metamorphism: an example from the US Cordillera. *Contrib. Mineral. Petrol.* 164, 521–536. <https://doi.org/10.1007/s00410-012-0751-7>
- Vogt-Vincent, N.S., Mitarai, S., 2020. A Persistent Kuroshio in the Glacial East China Sea and Implications for Coral Paleobiogeography. *Paleoceanogr. Paleoclimatology* 35. <https://doi.org/10.1029/2020PA003902>
- Wada, E., Hattori, A., 1976. Natural abundance of ^{15}N in particulate organic matter in the North Pacific Ocean. *Geochim. Cosmochim. Acta* 40, 249–251. [https://doi.org/10.1016/0016-7037\(76\)90183-6](https://doi.org/10.1016/0016-7037(76)90183-6)
- Walker, M., Johnsen, S., Rasmussen, S.O., Popov, V., Steffensen, J.-P., Gibbard, P., Hoek, W., Lowe, J., Andrews, J., Björck, S., Cwynar, L.C., Hughen, K., Kershaw, P., Kromer, B., Litt, T., Lowe, D.J., Nakagawa, T., Newnham, R., Schwander, J., 2009. Formal definition and dating of the GSSP (Global Stratotype Section and Point) for the base of the Holocene using the Greenland NGRIP ice core, and selected auxiliary records. *J. Quat. Sci.* 24, 3–17. <https://doi.org/10.1002/jqs.1227>
- Wan, S., Li, A., Clift, P.D., Stuu, J.-F.W., 2007. Development of the East Asian monsoon: Mineralogical and sedimentologic records in the northern South China Sea since 20 Ma. *Palaeogeogr. Palaeoclimatol. Palaeoecol.* 254, 561–582. <https://doi.org/10.1016/j.palaeo.2007.07.009>
- Wan, S., Tian, J., Steinke, S., Li, A., Li, T., 2010. Evolution and variability of the East Asian summer monsoon during the Pliocene: Evidence from clay mineral records of the South China Sea. *Palaeogeogr. Palaeoclimatol. Palaeoecol.* 293, 237–247. <https://doi.org/10.1016/j.palaeo.2010.05.025>
- Wan, S., Yu, Z., Clift, P.D., Sun, H., Li, A., Li, T., 2012. History of Asian eolian input to the West Philippine Sea over the last one million years. *Palaeogeogr. Palaeoclimatol. Palaeoecol.* 326–328, 152–159. <https://doi.org/10.1016/j.palaeo.2012.02.015>
- Wang, J., Li, A., Xu, K., Zheng, X., Huang, J., 2015. Clay mineral and grain size studies of sediment provenances and paleoenvironment evolution in the middle Okinawa Trough since 17ka. *Mar. Geol.* 366, 49–61. <https://doi.org/10.1016/j.margeo.2015.04.007>
- Wang, M., Liu, Z., Zhu, X., Yan, X., Zhang, Z., Zhao, R., 2019. Origin and formation of the Ryukyu Current revealed by HYCOM reanalysis. *Acta Oceanol. Sin.* 38, 1–10. <https://doi.org/10.1007/s13131-018-1329-7>
- Wang, Q., Song, J., Yuan, H., Li, X., Li, N., Wang, Y., 2018. Sources and burial of particulate organic matter in the Kuroshio mainstream and its response to climate change over

- the past millennium. *Geo-Mar. Lett.* 38, 497–511. <https://doi.org/10.1007/s00367-018-0551-9>
- Wei, K.-Y., Mii, H.-S., Huang, C.-Y., 2005. Age Model and Oxygen Isotope Stratigraphy of Site ODP1202 in the Southern Okinawa Trough, Northwestern Pacific. *Terr. Atmospheric Ocean. Sci.* 16, 001. [https://doi.org/10.3319/TAO.2005.16.1.1\(OT\)](https://doi.org/10.3319/TAO.2005.16.1.1(OT))
- Wu, C., Fu, F.-X., Sun, J., Thangaraj, S., Pujari, L., 2018. Nitrogen Fixation by Trichodesmium and unicellular diazotrophs in the northern South China Sea and the Kuroshio in summer. *Sci. Rep.* 8, 2415. <https://doi.org/10.1038/s41598-018-20743-0>
- Wu, C.-R., Chang, Y.-L., Oey, L.-Y., Chang, C.-W.J., Hsin, Y.-C., 2008. Air-sea interaction between tropical cyclone Nari and Kuroshio. *Geophys. Res. Lett.* 35. <https://doi.org/10.1029/2008GL033942>
- Xu, K., Milliman, J.D., Yang, Z., Xu, H., 2007. Climatic and Anthropogenic Impacts on Water and Sediment Discharges from the Yangtze River (Changjiang), 1950–2005, in: Gupta, A. (Ed.), *Large Rivers*. John Wiley & Sons, Ltd, Chichester, UK, pp. 609–626. <https://doi.org/10.1002/9780470723722.ch29>
- Xu, Z., Li, T., Clift, P.D., Lim, D., Wan, S., Chen, H., Tang, Z., Jiang, F., Xiong, Z., 2015. Quantitative estimates of Asian dust input to the western Philippine Sea in the mid-late Quaternary and its potential significance for paleoenvironment: ASIAN DUST INPUT TO WPS IN QUATERNARY. *Geochem. Geophys. Geosystems* 16, 3182–3196. <https://doi.org/10.1002/2015GC005929>
- Xu, Z., Li, T., Clift, P.D., Wan, S., Lim, D., Chang, F., Sun, R., 2019. Sea-level, monsoonal, and anthropogenic impacts on the millennial scale variability of siliciclastic sediment input into the western Philippine sea since 27 ka. *J. Asian Earth Sci.* 177, 250–262. <https://doi.org/10.1016/j.jseaes.2019.04.001>
- Xu, Z., Wan, S., Colin, C., Li, T., Clift, P.D., Chang, F., Sun, R., Yu, Z., Lim, D., 2020. Enhanced terrigenous organic matter input and productivity on the western margin of the Western Pacific Warm Pool during the Quaternary sea-level lowstands: Forcing mechanisms and implications for the global carbon cycle. *Quat. Sci. Rev.* 232, 106211. <https://doi.org/10.1016/j.quascirev.2020.106211>
- Yamamoto, M., 2009. Response of mid-latitude North Pacific surface temperatures to orbital forcing and linkage to the East Asian summer monsoon and tropical ocean-atmosphere interactions: response of North Pacific SST to orbital forcing. *J. Quat. Sci.* 24, 836–847. <https://doi.org/10.1002/jqs.1255>
- Yanase, W., Abe-Ouchi, A., 2007. The LGM surface climate and atmospheric circulation over East Asia and the North Pacific in the PMIP2 coupled model simulations. *Clim. Past* 3, 439–451. <https://doi.org/10.5194/cp-3-439-2007>
- Yang, Z., Li, T., Lei, Y., Chang, F., Nan, Q., 2020. Vegetation evolution-based hydrological climate history since LGM in southern South China Sea. *Mar. Micropaleontol.* 156, 101837. <https://doi.org/10.1016/j.marmicro.2020.101837>
- Yu, S.-W., Tsai, L.L., Talling, P.J., Lin, A.T., Mii, H.-S., Chung, S.-H., Horng, C.-S., 2017. Sea level and climatic controls on turbidite occurrence for the past 26kyr on the flank of the Gaoping Canyon off SW Taiwan. *Mar. Geol.* 392, 140–150. <https://doi.org/10.1016/j.margeo.2017.08.011>
- Yui, T.-F., Kao, S.-J., Wu, T.-W., 2009. Nitrogen and N-isotope variation during low-grade metamorphism of the Taiwan mountain belt. *Geochem. J.* 43, 15–27. <https://doi.org/10.2343/geochemj.1.0003>

- Zhang, H., Liu, C., Jin, X., Shi, J., Zhao, S., Jian, Z., 2016. Dynamics of primary productivity in the northern South China Sea over the past 24,000 years: productivity in the South China Sea. *Geochem. Geophys. Geosystems* 17, 4878–4891. <https://doi.org/10.1002/2016GC006602>
- Zhang, R., Chen, M., Cao, J., Ma, Q., Yang, J., Qiu, Y., 2012. Nitrogen fixation in the East China Sea and southern Yellow Sea during summer 2006. *Mar. Ecol. Prog. Ser.* 447, 77–86. <https://doi.org/10.3354/meps09509>
- Zhao, D., Wan, S., Toucanne, S., Clift, P.D., Tada, R., Révillon, S., Kubota, Y., Zheng, X., Yu, Z., Huang, J., Jiang, H., Xu, Z., Shi, X., Li, A., 2017. Distinct control mechanism of fine-grained sediments from Yellow River and Kyushu supply in the northern Okinawa Trough since the last glacial. *Geochem. Geophys. Geosystems* 18, 2949–2969. <https://doi.org/10.1002/2016GC006764>
- Zhao, Y., Liu, Z., Colin, C., Xie, X., Wu, Q., 2011. Turbidite deposition in the southern South China Sea during the last glacial: Evidence from grain size and major elements records. *Chin. Sci. Bull.* 56, 3558–3565. <https://doi.org/10.1007/s11434-011-4685-7>
- Zhao, Y., Zou, X., Liu, Q., Wang, C., Ge, C., Xu, M., 2018. Clay mineralogy indicates the muddy sediment provenance in the estuarine-inner shelf of the East China Sea. *J. Asian Earth Sci.* 152, 69–79. <https://doi.org/10.1016/j.jseaes.2017.11.036>
- Zheng, L.-W., Hsiao, S.S.-Y., Ding, X.-D., Li, D., Chang, Y.-P., Kao, S.-J., 2015. Isotopic composition and speciation of sedimentary nitrogen and carbon in the Okinawa Trough over the past 30 ka. *Paleoceanography* 30, 1233–1244. <https://doi.org/10.1002/2015PA002782>
- Zheng, X., Li, A., Kao, S., Gong, X., Frank, M., Kuhn, G., Cai, W., Yan, H., Wan, S., Zhang, H., Jiang, F., Hathorne, E., Chen, Z., 2016. Synchronicity of Kuroshio Current and climate system variability since the Last Glacial Maximum. *Earth Planet. Sci. Lett.* 452, 247–257. <https://doi.org/10.1016/j.epsl.2016.07.028>
- Zhou, Y., Chen, F., Wu, C., Yu, S., Zhuang, C., 2016. Palaeoproductivity linked to monsoon variability in the northern slope of the South China Sea from the last 290 kyr: evidence of benthic foraminifera from Core SH7B. *Geol. Soc. Lond. Spec. Publ.* 429, 197–210. <https://doi.org/10.1144/SP429.10>
- Ziegler, M., Jilbert, T., de Lange, G.J., Lourens, L.J., Reichert, G.-J., 2008. Bromine counts from XRF scanning as an estimate of the marine organic carbon content of sediment cores. *Geochem. Geophys. Geosystems* 9. <https://doi.org/10.1029/2007GC001932>
- Zou, J., Chang, Y.-P., Zhu, A., Chen, M.-T., Kandasamy, S., Yang, H., Cui, J., Yu, P.-S., Shi, X., 2021. Sedimentary mercury and antimony revealed orbital-scale dynamics of the Kuroshio Current. *Quat. Sci. Rev.* 265, 107051. <https://doi.org/10.1016/j.quascirev.2021.107051>

Declaration of interests

The authors declare that they have no known competing financial interests or personal relationships that could have appeared to influence the work reported in this paper.

The authors declare the following financial interests/personal relationships which may be considered as potential competing interests:

Journal Pre-proof

Highlights

- The Kuroshio Current deflected partially eastward during the LGM and HS1
- The Kuroshio Current exerts a strong control on the dispersion of hypopycnal flows
- Dust and upwelled nutrients under intensified EAWM control paleoproductivity
- Intensified primary productivity in the NW Philippine Sea during the LGM and HS1

Journal Pre-proof